Table of Contents for Chapter 9

9. 1 Overview 3
9.1.1 Introduction 3
9.1.2 Overview of Research Thrusts 5
9.1.2.1 Thrust ASC-1: Scenario Development 5
9.1.2.2 Thrust ASC-2: Axisymmetric Control Development 6
9.1.2.3 Thrust ASC-3: Disruption Avoidance By Controlled Discharge Shutdown 7
9.1.2.4 Thrust ASC-4: Scenario Optimization for Next Step Devices 7
9.1.2.5 Thrust Connections to Research Described in Other Chapters 8
9.2 Research Plans For Advanced Scenarios and Control 8
9.2.1 Thrust 1: Scenario Development of NSTX-U 8
9.2.1.1: 100 % Non-Inductive Scenarios 9
9.2.1.1.1: Research Description 9
9.2.1.1.2: Research Plans by Year 13
9.2.1.2: Long-Pulse Partial Inductive Operations 14
9.2.1.2.1: Research Description 14
9.2.1.2.2: Research Plans by Year 20
9.2.1.3: RF Heating for Advanced Scenarios 21
9.2.1.4: Coupling to Non-Inductive Startup and Ramp-Up 22
9.2.1.5: Impact of High-Z PFC Conversion on Scenario Development 23
9.2.2 Thrust 2: Axisymmetric Control Development 23
9.2.2.1: Overview of Control Development 23
9.2.2.2: Advanced Boundary and Position Control 24
9.2.2.2.1: Realtime Equilibrium Reconstruction and Boundary Control 24
9.2.2.2.2: Vertical Position Control 26
9.2.2.2.3: Research Plans by Year 28
9.2.2.3: Closed Loop Control of Divertor Magnetic Geometry and Radiation 29
9.2.2.3.1: Snowflake Divertor Control 29
9.2.2.3.2: Radiative Divertor Control 31
9.2.2.3.3: Research Plans By Year 32
9.2.2.4: Profile Control 33
9.2.2.4.1: Safety-Factor Profile Control 33
9.2.2.4.2: Rotation Profile Control 37
9.2.2.4.3: Collaborations in Profile Control 39
9.2.2.4.4: Research Plans by Year 40
9.2.2.5: Deuterium Inventory Control 41
9.2.2.5.1: Realtime Density Measurements 41
9.2.2.5.2: Conventional Gas Injectors 41
9.2.2.5.3: Supersonic Gas Injectors 42
9.2.2.5.4: Pumping Schemes 43
9.2.2.5.5: Deuterium Inventory Control Plans 44

9.2.2.5.6: Research Plans by Year 44
9.2.3 Thrust 3: Disruption Avoidance By Emergency Stop Development 45
9.2.3.1 Realtime Determination of Need for Discharge Termination 45
9.2.3.1.1: Engineering Indicators 45
9.2.3.1.2: Data-Based Disruption Indicators 46
9.2.3.1.3: Physics-Based Disruption Indicators 49
9.2.3.2: Soft- and Hard-Stop Sequence Development 49
9.2.3.3: Research Plans By Year 51
9.2.4 Thrust 4: Exploration of Scenario Physics of Next Step STs 51
9.2.4.1: Optimal Profiles for High-β_N Steady State 51
9.2.4.1.1: Research Description 51
9.2.4.1.2: Research Plans by Year 53
9.2.4.2: Range of Validity for Classical Neutral Beam Current Drive Calculations 53
9.2.4.2.1: Research Description 53
9.2.4.2.2: Research Plans by Year 55
9.2.4.3: Exploration and Validation of Integrated Models for FNSF and other Next-Step STs 56
9.3 Simulation Tools for Integrated Scenario Research and Control Development 58
9.3.1: TRANSP 58
9.3.2: DCON 58
9.3.3: TOKSYS 58
9.3.4: EFIT & LRDFIT: 58
9.3.5: NUBEAM 58
9.3.6: Other Codes 59
9.4 Research Timeline 59
References 61

Chapter 9

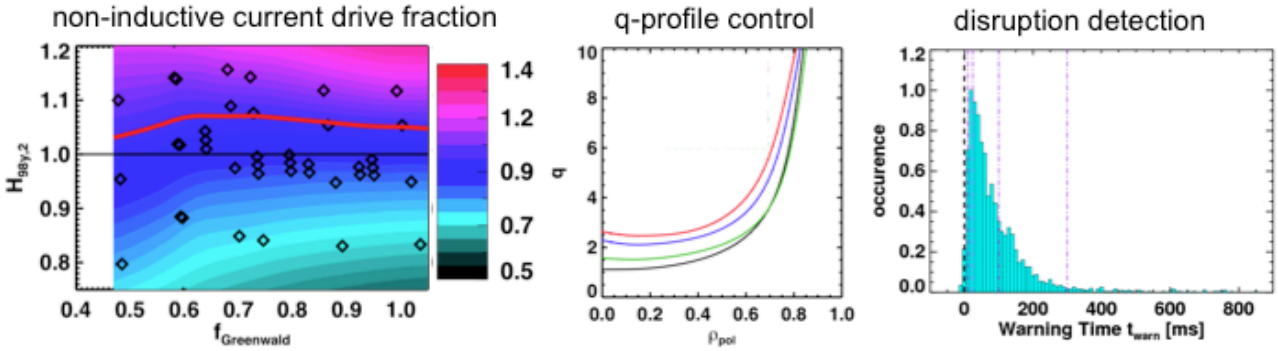

Research Goals and Plans for Plasma Sustainment: Advanced Scenarios and Control

9. 1 Overview

9.1.1 Introduction

As described in Chapter #1, the ST has been suggested for use as the fusion core of Fusion Nuclear Science Facilities (FNSFs) [1-3] and Component Test Facilities (CTFs) [4], pilot power plants [5], and even full-scale power reactors [6,7]. While there is a range of operating points suggested for these next step spherical torus devices, they have many features in common.

As shown in Fig. 9.1a), these next-step STs generally operate with β_N>4, exceeding the no-wall n=1 kink stability limit and requiring optimization of the passive and active stability. The values of boundary elongation, illustrated in Fig. 9.1b), are typically quite high, generally exceeding 2.5. These high values of β_N and elongation contribute to a large fraction of the required current being driven by the bootstrap effect. These devices generally rely on neutral beam current drive (NBCD) to supplement the bootstrap current, in order to maintain 100% non-inductive current drive. They all have potentially very high power loading of the divertor, and so heat flux mitigation strategies are required. Finally, they all must have a much lower rate of unmitigated disruptions than achieved in current low and high aspect ratio tokamaks, in order to avoid plant damage and the loss of valuable discharge time.

Scenario development research in NSTX made considerable progress toward achieving these goals [8], as evidenced by the TRANSP analysis of NSTX data in Fig. 9.1. The data points are averages of durations longer than τ_E during stationary periods of high-performance discharges. Fig. 9.1a) demonstrates that values of β_N in excess of 6 have been achieved for substantial durations, with values above 4 quite common. Elongations up to 2.9 were similarly achieved. However, the evolution of the current, rotation, and density profiles during the discharge typically resulted in deviations from the optimal conditions, often leading to disruption. Furthermore, the maximum non-inductive fraction ever achieved in NSTX was 65-70% [8-10].

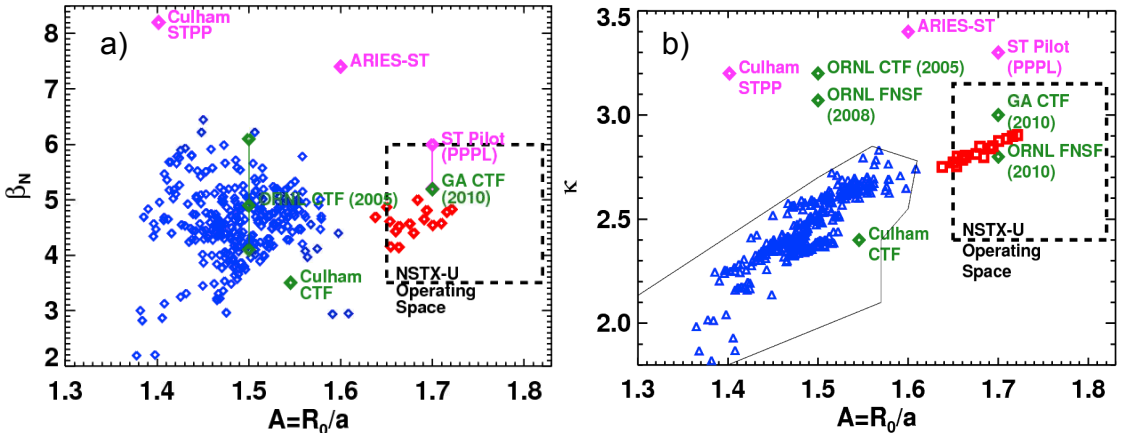

Fig. 9.1) Comparison of the NSTX operating space to the proposed steady state solutions for fusion nuclear science facilities, component test facilities, and power generating facilities. NSTX data from a dedicated higher aspect ratio experiment is shown in red, while the remainder of an NSTX high-performance database is shown in blue.

Based on the NSTX experience and R&D needs for next step devices, the following overarching questions guide the scenario and control research plans in NSTX-U [11]:

- What are the optimal current and rotation profiles for achieving a 100% non-inductive state?
- What are the optimal control strategies for maintaining those profiles?
- Under what conditions can neutral beam current drive be understood using neoclassical theory alone?
- Can the divertor heat flux be controlled in a fashion consistent with a high-performance plasma core?
- How can impending disruptions be detected, and what are the optimal discharge termination responses?
- How can NSTX-U results be used to project to next-step STs?

In order to make progress on these important problems, research in the Advanced Scenarios and Control (ASC) topical science group will be divided into four thrusts. The first thrust will focus on scenario development and optimization using the NSTX-U actuators; this thrust will demonstrate 100% non-inductive operating points as well as develop high-current partial-inductive scenarios for the use by other topical science groups. The second thrust will focus on axisymmetric control development, including profile and divertor control. The third thrust will focus on the controlled termination of high-β_N ST discharges, including disruption detection and intervention. The fourth thrust will examine critical issues related to scenario development for next-step STs, including regimes of classical beam current drive and transport modeling. As described in Section 9.1.2, these thrusts are entirely supportive of the five high-level goals for the NSTX-U research program defined in Section 1.2.2.

Finally, note that while these research goals are framed in terms of next-step ST needs, the physics and technology issues are very relevant to the problems facing ITER. An incomplete list overlapping research tasks includes:

- ITER will rely on off-axis neutral beam current drive in its advanced scenarios, and so improving the understanding of NBCD, including the range of validity of neoclassical treatments and its use as a control actuator, is critical.
- ITER will rely on profile control to maintain a stable operating scenario. The development of robust algorithms for that control is thus critical.
- ITER modeling has and will continue to rely on reduced transport models for predicting scenario characteristics. Benchmarking these models on the widest possible range of scenarios, including STs, increases the confidence in those predictions.
- ITER will need to radiate a large fraction of the power that crosses into the SOL, in order to avoid damage to the divertor places. Closed loop radiative divertor control research in NSTX-U can aid in developing the appropriate control for ITER.
- ITER will need to trigger its disruption mitigation systems based on realtime diagnostics, and this research can aid in developing the appropriate trigger algorithms.

9.1.2 Overview of Research Thrusts

9.1.2.1 Thrust ASC-1: Scenario Development

This thrust will focus on developing the highest-performance scenarios possible in NSTX-U. Broadly speaking, there are two types of optimization to be considered in this research thrust: 100 % non-inductive current drive and high current partial inductive.

The first optimization aims at 100% non-inductive current drive scenarios at the largest possible currents. Key questions to be examined are the impact of plasma transport and the resulting

profile shapes on the non-inductive current level, the global stability of these scenarios with large neutral beam current drive and central fast ion pressures, the optimal density for non-inductive sustainment, and consistency of the non-inductive operating state with divertor integration. The research of this first optimization activity provides the basis for achieving the highest priority research goal #1 of the 5 year plan in Chapter 1: Demonstrate stationary 100% non-inductive operation at performance that extrapolates to ≥ 1MW/m2 neutron wall loading in FNSF.

The second optimization task will develop high-current, partial inductive operation, pushing toward the facility goal of 5 second pulses at I_P=2.0 MA and B_T=1.0T. These scenarios are the key means of accessing low collisionality in NSTX-U, and the development of lower-density operations is thus critical. Additionally, it is likely that these scenarios will result in severe divertor thermal loading, and so the development of integrated heat flux management solutions is a requirement.

Overall, this thrust supports all five of the high-level NSTX-U goals described in Section 1.2.2, and will be described in detail in section 9.2.1.

9.1.2.2 Thrust ASC-2: Axisymmetric Control Development

This thrust will focus on developing the control strategies for achieving and maintaining optimal ST scenarios. Maintaining the plasma boundary shape and vertical position may be the most basic tokamak control requirement, and NSTX-U research will optimize multi-input multi-output boundary shape controllers and improved vertical stability algorithms. This is a critical issue for the ST, where inboard coils for maintaining the inner gap may not be available and very high elongations are desired.

In addition to the boundary shape, control of the divertor heat flux is critical. The snowflake divertor [12,13], which uses two or three divertor coils to pull nearly overlapping X-points, has been shown to lead to a significant reduction in the divertor heat flux in NSTX [14,15] and DIII-D [16]. NSTX-U researchers will work to develop realtime tracking of multiple X-points. This information will be used to develop closed-loop control of the 1st and 2nd X-point locations, and this control will be incorporated into advanced scenarios. Furthermore, direct control of the divertor radiation using feedback control of impurity gas injection will be developed, based on earlier success with open-loop detached divertor experiments [17,18].

The safety factor and rotation profile shapes play a key role in determining the global transport and stability levels. TRANSP calculations show that by varying the neutral beam source mix and/or plasma density, the minimum safety factor (q_{min}) can be controlled; experiments will be conducted to verify this prediction. These results will be used to develop simultaneous β_N and

q_{min} controllers in NSTX. Similarly, the variation of neutral beam torques from the different sources and n=2 & 3 magnetic braking from the RWM coils will be used to control β_N and the values of toroidal rotation at selected points across the profile. Finally, experiments will attempt to examine the feasibility of combined control, for instance, simultaneous β_N, q_{min}, & $F_{T,0}$ control (here, $F_{T,0}$ represents the central rotation frequency).

Finally, it will be important to develop means to control the particle inventory. Realtime density measurements will be brought to the plasma control system (PCS), and improved fueling actuators will be developed. When added to the pumping produced by lithium coatings or a cryo-pump, these tools will provide a means of generating a controlled density evolution in NSTX-U.

This thrust also supports all five of the high-level NSTX-U goals described in Section 1.2.2, and will be described in detail in section 9.2.2.

9.1.2.3 Thrust ASC-3: Disruption Avoidance By Controlled Discharge Shutdown

All tokamak discharges must end, either in controlled rampdown or in disruption. The purpose of this thrust is to optimize disruption detection with sufficient time to make a meaningful intervention. Realtime inspection of quantities like the coil heating and the solenoid flux evolution will be used to determine when slow rampdowns will be required. Multiple realtime diagnostic signals will be synthesized to form efficient disruption detectors, requiring more rapid rampdowns.

This information will be used to trigger automated rapid rampdown sequences. It is envisioned that multiple types of rampdown sequences will be developed, pending the different sources of alarms. A massive gas injection (MGI) sequence will also be included, to take advantage of the MGI system being developed in the MS TSG as described in Chapter 2.

This thrust supports the first two high-level NSTX-U goals described in Section 1.2.2, and will be described in detail in section 9.2.3.

9.1.2.4 Thrust ASC-4: Scenario Optimization for Next Step Devices

As noted above, Thrusts 1-3 aim to optimize the discharges given the facility constraints of NSTX-U. Thrust 4 will study aspects of scenario optimization physics relevant to next-step devices, in ways that may not produce optimized scenarios for NSTX-U. For instance, the simultaneous current and rotation profiles providing optimal performance will be examined. The conditions for classical beam current drive will be explored. Finally, integrated modeling of the

thermal energy, toroidal rotation, and current will be pursued, first for validation against NSTX-U results, and then for projection to next-step ST scenarios.

This thrust supports the first two high-level NSTX-U goals described in Section 1.2.2, and will be described in detail in section 9.2.4.

9.1.2.5 Thrust Connections to Research Described in Other Chapters

The thrusts in this chapter are not only related to each other, but also both build on and support the research described in other chapters. A non-exhaustive list of examples include:

- This research is directly coupled to macrostability thrust MS-3 on disruption dynamics, detection, mitigation and avoidance. In particular, the massive gas injection research described there will utilize the disruption detector research described in thrust ASC-3, while techniques developed in that ASC thrust will provide the trigger for MGI.
- Research in Transport and Turbulence thrusts TT-1 on global confinement scaling and TT-3 on reduced transport models will contribute directly to understanding the optimal profiles for advanced scenario plasmas, as described in thrust ASC-4
- Progress in understanding the physics underlying the scaling and control of the divertor heat flux in Boundary Physics thrust BP-2 will be critical in executing thrusts ASC-1 and ASC-2.
- The understanding of neutral beam current drive required to execute thrusts ASC-1, -2 and -4 will build on knowledge developed in thrust EP-1, dedicated to understanding *AE induced fast ion transport.
- The H-mode scenarios and control algorithms described in thrusts ASC-1 and ASC-2 may benefit from the use of HHFW heating, as described in Section 7.2.1.
- The knowledge of neutral beam current drive derived from the studies described in thrusts ASC-2 and ASC-4 will assist in the non-inductive ramp-up research described in the Solenoid-Free Start-Up thrusts.

9.2 Research Plans

9.2.1 Thrust 1: Scenario Development of NSTX-U

As implied by the name of the chapter, the development of high-performance operating scenarios for NSTX-U is a key goal of this research effort. These scenarios are important in their own right, but also as “laboratories” for physics studies in other topical science areas. This section describes plans for developing these scenarios, focusing on 100% non-inductive scenarios first, followed by high-current partial inductive scenarios.

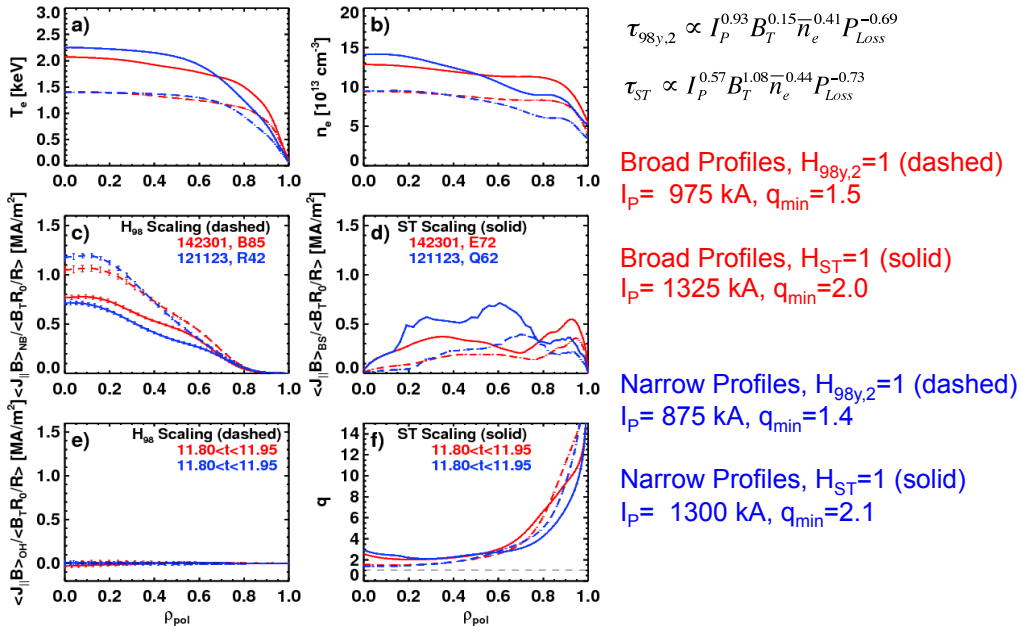

Fig. 9.2: Profiles of a) the electron temperature, b) the electron density, c) the neutral beam driven current, d) the bootstrap current, e) the loop voltage, and f) the safety factor. The colors correspond to different thermal profile shapes, while the line-style indicates the confinement level (dashed for H_{98}=1, and solid for H_{ST}=1).

9.2.1.1: 100 % Non-Inductive Scenarios

9.2.1.1.1: Research Description

Before addressing the development path for 100% non-inductive scenarios, it is useful to consider some of the key variables impacting these scenarios [19]. To begin with, the impact of the confinement level and profile shapes is shown with the simulations in Fig. 9.2. Fig. 9.2a) shows four electron temperature profiles, while Fig. 9.2b) shows four electron density profiles; the parameters defining these profiles will be defined below. The toroidal field is B_T=1.0 T for all these calculations, with an injected power of 12.6 MW from all six sources operating at 90 kV. The elongation is κ=2.8 in these cases, with high boundary triangularity, a condition known to maximize the core performance in NSTX [20,21]. The Greenwald fraction is 0.7 in all cases, with Z_{eff}=2. The plasma current has been chosen to yield a fully non-inductive operating point in all cases, and has been allowed to fully relax.

The two red curves correspond to broad density and temperature profiles, while the two blue curves come from discharges with more peaked profiles; these two profile sets bound the range of thermal pressure profile peaking observed in NSTX. The solid lines correspond to the assumption of an ST specific scaling expression for the thermal energy confinement [22] $\tau_{ST} = I_P^{0.57} B_T^{1.08} \bar{n}_e^{0.44} P_{Loss}^{-0.73}$, while the dashed lines correspond to the ITER-98$_{y,2}$ scaling expression: $\tau_{98(y,2)} = I_P^{0.93} B_T^{0.15} \bar{n}_e^{0.41} P_{Loss}^{-0.69} R_0^{1.97} \varepsilon^{0.58} \kappa^{0.78}$. It is anticipated that, in lieu of any validated thermal and particle transport models, these two profile and global confinement assumptions will bracket the operational point for this field, current, and power

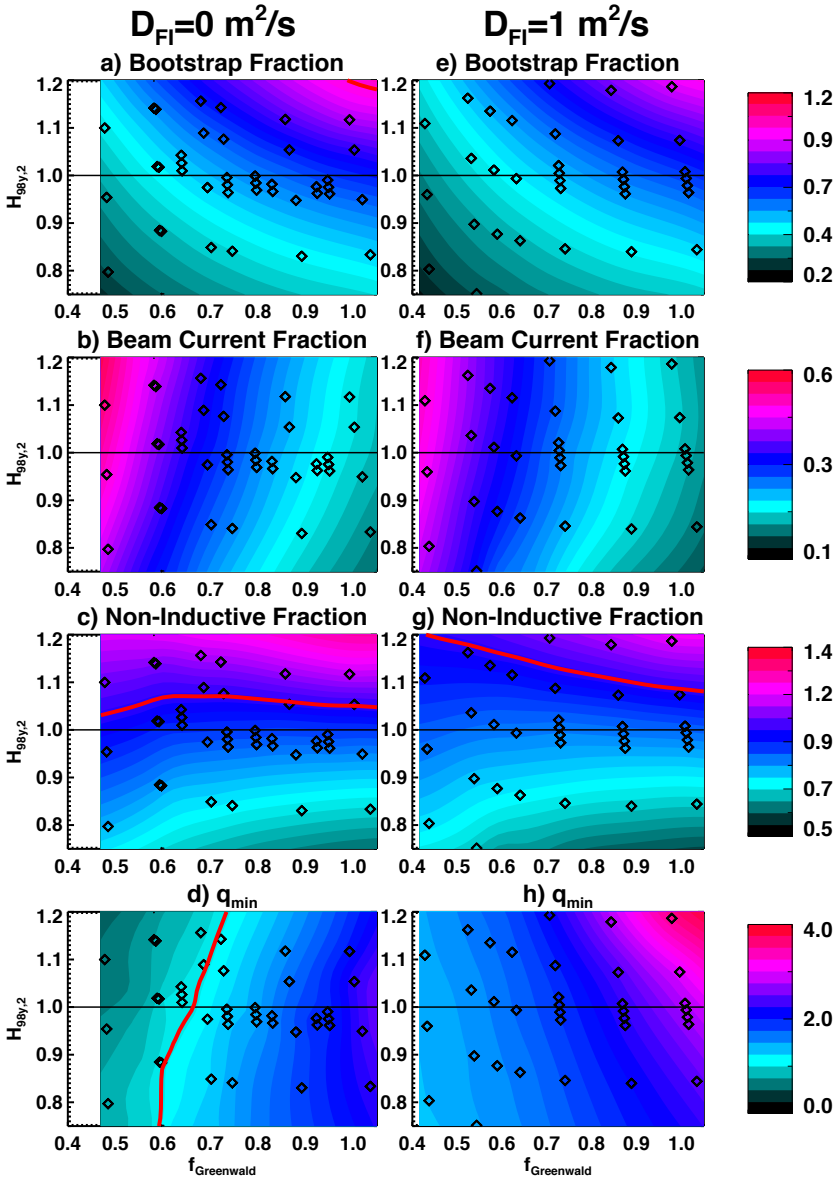

Fig. 9.3) Contours of bootstrap fraction, beam current drive fraction, non-inductive fraction, and q_{min}, as a function of the confinement multiplier and density. The left column is for classical beam physics, while the right column invokes a small level of fast-ion diffusion. The points are the underlying TRANSP simulations from which the contours are interpolated, and the red curves correspond to a non-inductive fraction of 1 or q_{min}=1.

With this background, a large number of trends can be observed in this figure. The most critical is that the non-inductive current level, for this toroidal field, boundary shape, injected power, and Greenwald fraction, is in the vicinity of 900-1000 kA for ITER-98 scaling, but ~1300 kA for the case with the ST specific thermal confinement scaling. This large difference is due to the different B_T scaling of confinement in the two expressions, with the strong B_T dependence of the ST scaling law having a strong impact. As a consequence of both the stronger B_T scaling and the increased non-

inductive level of plasma current, the central electron temperature for the H_{ST}=1 case is in the vicinity of 2.0-2.2 keV, while it does not exceed 1.5 keV for the case with ITER-98$_{y,2}$ scaling. Finally, the central safety factors are above 2 and have some reversed shear for the cases with ST thermal confinement scaling, while the ITER confinement scaling leads to the result of $q_{min}=q_0\sim1.5$. Hence, the difference between these two confinement scaling expressions, a critical question for projecting next-step ST operating points, should be quite visible when the non-inductive operating point is determined in NSTX-U.

A second variable key to determining the non-inductive operating point is the plasma density. Fig 9.3 shows how key parameters vary as a function of density and confinement level for a scenario with P_{inj}=12.6 MW, I_P=1.0 MA, B_T=1.0 T, and Z_{eff}=2. Consider the left column for now, where the calculations assume that the fast ion slowing down is classical.

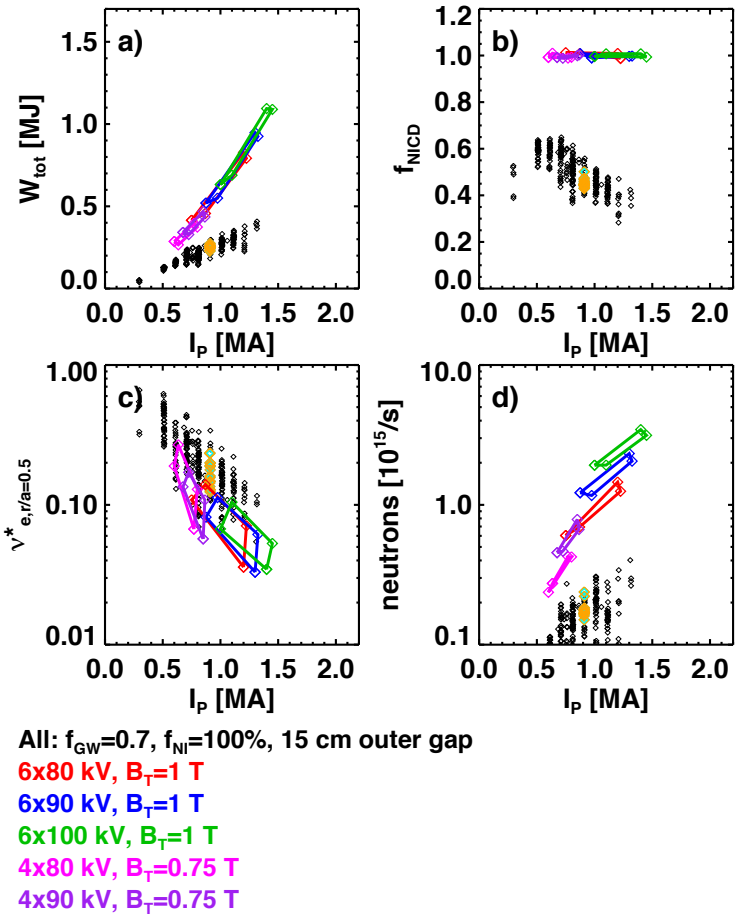

Fig. 9.4: Plots of a) the stored energy, b) the non-inductive current fraction, c) the mid-radius collisionality, and d) the neutron emission, as a function of the plasma current, for NSTX data and projected NSTX-U scenarios.

Fig 9.3a) shows the bootstrap fraction as a function of confinement and density; the bootstrap current increases with both confinement at fixed density, and with density at fixed confinement multiplier. The beam current drive fraction in frame 9.3b) increases with confinement, but decreases strongly with increasing density.

When these results are summed (along with the small contribution from Pfirsch-Schlueter and diamagnetic currents), the resulting non-inductive fraction is shown in Fig. 9.3c). Interestingly, the non-inductive fraction is largely independent of f_{GW} in this region of parameters space, and 100% non-inductive operations is achieved at $H_{98y,2}\approx1.04$.

The central safety factor, however, is a strong function of density in

this configuration. Beneath f_{GW}~0.6, the central safety factor tends to fall beneath unity, a situation guaranteed to result in disruptive core n=1 kink/tearing modes [9,23-27]. This is due to the strong neutral beam current drive at lower density, which tends to be peaked on the magnetic axis, as indicated in Fig. 9.2c). At higher densities, the NBCD is reduced, while the off-axis peaked bootstrap current contributes to an elevated central safety factor. Furthermore (not shown), the strong central peaking of the fast ion pressure at lower density results in the configuration becoming n=1 MHD unstable. Hence, it will likely be critical to avoid too-low a density in these scenarios; the caveat to this statement is shown in the right-hand column of Fig. 9.3, where a small level of fast ion diffusivity has been added to the simulation. These simulations with fast ion density included will be discussed in greater detail in Section 9.2.4.2.

Additional information about fully non-inductive scenarios in NSTX-U is given in Fig. 9.4. This figure shows the basic NSTX database in black points, and data from the dedicated high-A experiments in NSTX as orange points. Each of the colored shapes corresponds to a family of scenario simulations with the same toroidal field strength, boundary shape, and heating power; the four corners of each shape corresponding to the two confinement assumptions and the narrow and broad thermal profiles, as discussed in the context of Fig. 9.2. This figure will guide the description of the research plan given below.

B_T [T]	P_{inj} [MW]	Heating Pulse Duration [s]	I_P Range [kA]	τ_{CR} [s]
0.75	6.8	5.0	$600<I_P<800$	$0.3<\tau_{CR}<0.4$
0.75	8.4	3.0	$675<I_P<850$	$0.3<\tau_{CR}<0.45$
1.0	10.2	5.0	$750<I_P<1200$	$0.35<\tau_{CR}<0.75$
1.0	12.6	3.0	$875<I_P<1300$	$0.4<\tau_{CR}<0.8$
1.0	15.6	1.5	$1000<I_P<1450$	$0.4<\tau_{CR}<0.85$

Table 9.1: Selected parameters for 100% non-inductive scenarios at f_{GW}=0.7 in NSTX-U. See Table 2 and Appendix 1 of Ref. [19] for additional information.

As described in Section 10.7, the toroidal field for the first year of NSTX-U operations will be ≤ 0.8 T. The associated operating points for different heating powers are shown in Fig. 9.4 in magenta and purple, and in the first two rows of Table 9.1. The TRANSP simulations project the non-inductive currents to be in the range of $600 < I_P$ [kA] < 800. The goal for the first year operations (2nd year of the plan) will be to demonstrate these operating points for short periods, for instance, a few τ_E. In the second year of operations, research will attempt to extend these scenarios at 0.75 T to a few τ_{CR}.

In the second year of operation, shorter pulses at B_T=1.0 T will be available, and it is envisioned that from the third year on, full-field (B_T=1.0 T) operation will be allowed with full 5 second

flat-top durations. The details of these scenarios are illustrated in the red, blue, and green curves of Fig. 9.4, and the lower three rows of Table 9.1. It can be seen that these scenarios project to higher stored energy and larger neutron emission than any scenarios achieved in NSTX; the collisionality of these scenarios, which are not designed to reduce this parameter, is comparable to the lowest achieved in NSTX. Some run-time will be dedicated to develop short-duration 100% non-inductive scenarios at B_T=1.0 T in the 2nd operations year, using 90-100 kV beams to increase the current level. These 100 % non-inductive scenarios at 1.0T will be extended to the full 5-second flat-top in the later years, using 80 kV beams.

Lack of particle control is a potential barrier to completing these plans for long-pulse fully non-inductive operations; this will be addressed in the following way. The divertor cryo-pump does not come online until the third year of NSTX-U operations. During the period before the pump is installed, both boronization and lithium technologies will be explored to facilitate density and impurity control. For instance, it is possible that ELMs triggered by the lithium granule injector can be used to reduce the impurity accumulation. Alternatively, ELM pacing by 3-D fields can be explored. Additional discussion of these particle control techniques will be given in section 9.2.1.2 and 9.2.2.4, as well as in the boundary physics chapter.

During the final two years of the research program, additional attention will be given to integrating the 100% non-inductive operating point with other discharge goals. One goal will be to maximize the non-inductive current level at 1.0 T and high β_N. These studies will benefit from stability and profile optimization studies to be conducted in collaboration with the Macro Stability (MS) group. Another such integration step will be to add advanced-geometry or radiating divertors to the configurations; these scenarios may not require active heat flux mitigation, but testing their compatibility with those mitigation techniques will have value. Experiments will also begin to integrate the high-performance non-inductive flat-top scenarios with non-inductive current ramp-up research. This integration will be described in section 9.2.1.4.

9.2.1.1.2: Research Plans by Year

The plans and goals for this research topic can be summarized as:

Year 1 of operations (2015):

- Develop very high non-inductive fraction discharges at 600< I_P [kA]<800 at B_T=0.75, for a few τ_E.

Year 2 of operations (2016):

- Extend the duration of the very high non-inductive fraction at B_T=0.75 T to a τ_{CR} or longer.

- Utilize higher toroidal fields up to B_T=1.0 T to achieve 100% non-inductive at higher I_P levels for short pulse.

Year 3-4 of operations (2017-2018):

- Extend the duration of fully non-inductive currents to the full five second beam heating pulse, including optimization of particle control with the cryo-pump.
- Integrate 100% non-inductive scenarios with advanced divertor solutions.
- Integrate 100% non-inductive scenarios with non-inductive ramp-ups.

9.2.1.2: Long-Pulse Partial Inductive Operations

9.2.1.2.1: Research Description

In addition to the 100% non-inductive goal described in the previous section, the NSTX-U program has a goal of achieving long pulse with controlled density and higher current, up to I_P=2.0 MA. Scientific motivations for this scenario goal include:

- Testing the I_P scaling of core transport and the SOL width.
- Accessing low collisionality for core transport and global stability studies.
- Testing long-pulse disruption avoidance for many current redistribution times.

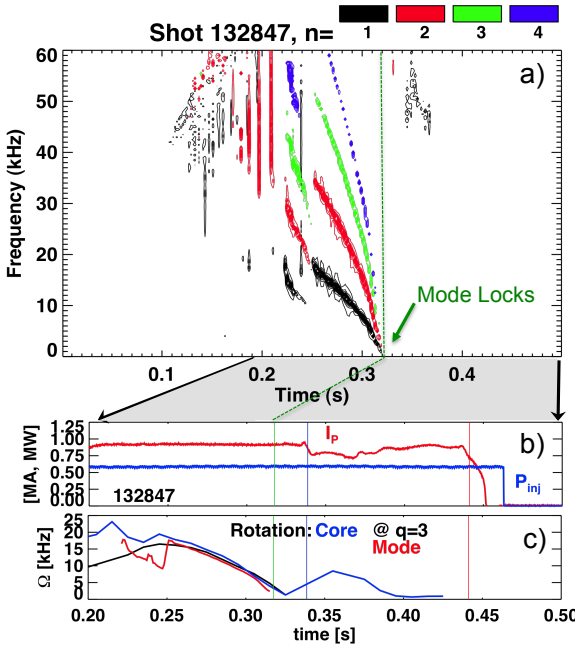

Fig. 9.5: Example dynamics of a discharge with incorrect early fueling. Shown are a) a spectrogram decomposed by toroidal mode number, b) the plasma current and heating power, and c) the core, q=3 surface, and mode rotation frequencies.

Accessing low collisionality is most easily done at lower density, since the normalized collisionality scales as $\nu^* \propto \frac{f_{GW}^3}{B_T \beta_N^2}$ at fixed β_N and toroidal field (it is assumed here that sufficient heating power is available to heat to the β-limit at any Greenwald fraction). β_N is limited by transport and/or global stability, and B_T is limited to 1.0 T in NSTX-U. Thus, reducing f_{GW} is the best means to reduce the collisionality. However, achieving sustained low density in NSTX has proven to be quite difficult, for two reasons:

- the requirement to provide strong fueling during the early phase of the discharge,
- the continued rise of the electron

density during the H-mode phase.

These two issues will be discussed below.

When insufficient fueling is provided at the beginning of the discharge, a wide variety of disruptive MHD activity has been observed to occur. A single example of this activity is shown in Fig. 9.5, where the MHD activity associated with an incorrectly fuelled discharge is illustrated [27]. In this case, a large n=1 mode strikes at t~0.24, and rapidly spins down to zero frequency. The disruption follows rapidly after the mode locks to the wall. Disruptions of this type are typically eliminated by increasing the fueling, often from the high-field side gas injector. This fueling modification does not prevent the early MHD modes from developing, but rather prevents them from spinning down to zero frequency; their frequency tends to saturate at 5-15 kHz in these non-disruptive cases, while their amplitude decays over a period of ~100-200 ms [27].

Experiments will explore a number of options for eliminating these and other disruptive MHD modes from discharges with reduced fueling during the first two years of NSTX-U operations. One hypothesis is that the extra gas fueling cools the plasma edge, resulting in more rapid current penetration and avoidance of the most unstable current profiles. The present fast ramps in NSTX were designed to provide the longest possible I_P flat-top for the rather modest flux capabilities of that solenoid. Given the larger flux of the NSTX-U solenoid, most scenarios are projected to tolerate greater flux consumption during the I_P ramp. Hence, the impact of ramping the plasma current more slowly will be examined. The gas fueling and I_P ramp rate will be scanned, to determine the optimal combination for achieving stable flat-top configurations at reduced density. The feedback-control of the line-average density described in section 9.2.2.4, when available, will be very beneficial for this study.

Beyond the I_P ramp rate, other means of achieving reduced density at the end of the ramp-up phase will be explored. Given that modes locking to the vessel wall precede many of these disruptions, experiments will investigate whether new error-field correction strategies in the early part of the discharge can improve the discharges. The dominant source of n=1 error-field in NSTX was from the tilting of the toroidal field coil due to interaction with stray field from the OH solenoid connections [28]. These OH connections have been i) moved from the top of the coil in NSTX to the bottom of the coil in NSTX-U, and ii) replaced with a coaxial design with smaller stray fields [11]. It is anticipated that these two changes will dramatically reduce error fields during the startup phase, but a new error field assessment must be performed as described in Chapter 2. Experiments will also examine whether use of more tangential neutral beam sources can result in greater rotation of the plasma, potentially preventing modes from locking to the wall.

Regardless of whether the density at the start of flat-top was f_{GW}=0.2 or f_{GW}=0.6, NSTX discharges tended to have a ramping electron density evolution. In ELMy H-mode with boron coatings of the plasma facing components, this increasing density was due to the accumulation of deuterium in the plasma. In ELM-free conditions with lithium-coated PFCs, the ramping electron density was typically due to the accumulation of carbon; as described in section 9.2.2.4, the deuterium inventory was often well controlled in those discharges. Research in the first years of NSTX-U will, in conjunction with the boundary physics and M&P research plans described in Chapters 4 and 5, attempt to stop the density rise by the following means:

- In cases with boronized PFCs, natural ELMs will be used to provide impurity control. The deuterium supplied to the plasma will be minimized via careful optimization of the plasma startup phase.

- In ELM-free lithium-conditioned discharges, the lithium granule injector will be used to attempt both lithium replenishment and ELM pacing. It is anticipated that this combination will provide both the good confinement of lithium-conditioned H-modes and the impurity transport of an ELMy regime.

- If this method fails, then experiments will be conducted to optimize magnetic ELM pacing with non-axisymmetric fields [29], for control of the impurity inventory in lithium-conditioned H-modes. In this case, the key task will be to maintain the desired impurity flushing properties without inducing large rotation damping or MHD modes.

- There is evidence that regimes with modest lithium conditioning may provide some confinement improvement without eliminating ELMs. Research will explore these regimes, with the goal of determining whether some small amount of lithium conditioning can provide deuterium pumping while not suppressing ELMs.

- ELM pacing with vertical jogs [30] may be used in advanced scenarios if the previous methods fail.

- Most NSTX H-mode discharges used fueling from a high field side (HFS) gas value to induce H-mode. This gas was injected down a long tube, and continued to flow into the plasma long after the H-mode transition. NSTX-U research will attempt to replace this fueling with that from injectors with more rapid time-response, namely the center-stack “shoulder” injector, and outboard supersonic gas injectors. See section 9.2.2.4 for more information on these fueling studies.

It is anticipated that the cryo-pump will be available between the 2nd and 3rd years of operations. Once this pump is installed and commissioned, it will, as described in the boundary physics chapter 4, be used to investigate density control in these higher current NSTX-U scenarios. See section 4.2.3 for additional information on the physics design of the cryo-pump system.

In addition to achieving density control, a second critical requirement will be to incorporate feedback controlled heat flux mitigation strategies into high-current and high-power scenarios. It is anticipated that this work will begin in the third year of the research program. The magnitude of the issue can be seen from Table 9.2, which describes the peak heat flux and time for the tile surface to reach T_{max}=1200°C, as a function of heating power, plasma current, and flux expansion. The temperature limit of 1200°C was selected here, as radiation induced sublimation has been observed above this temperature [31]. Additionally, the horizontal target tiles have been qualified for an average heat flux of 5 MW/m^2 for five seconds, with the limit being due to internal thermal stresses. In evaluating the tile heating for NSTX-U scenarios, the following assumptions have been made: the midplane scrape-off layer heat flux scales as $\lambda[mm] = 9.2 I_P^{-1.6}$, the peak heat flux scales as $Q_{Pk} = \frac{P_{loss} f_{div}}{2\pi R_{OSP} \lambda_q f_{\exp}}$, and that the time dependence of the surface temperature varies as $T_{surf} = 90 Q_{avg} \sqrt{t}$ [32], with $Q_{avg} = Q_{Pk}\left(1 - e^{-1}\right)$. Here, f_{div} is the fraction of the input power reaching each divertor, with f_{div}=0.4 implying that 80% of the input power enters the SOL, and that it is split evenly between the upper and lower divertors with no radiation in the divertor itself. f_{exp} is the flux expansion at the outer strikepoint, with values of 15 typical for standard divertors in NSTX-Upgrade.

				f_{exp}=15, f_{div}=0.4, T_{max}=1200 C		f_{exp}=60, f_{div}=0.4, T_{max}=1200 C or f_{exp}=15, f_{div}=0.1, T_{max}=1200 C	
Case	I_P (MA)	P_{inj} (MW)	Heating Pulse Duration [s]	Q_{PK} [MW/m^2]	Time to T_{max} [s]	Q_{Pk} [MW/m^2]	Time to T_{max} [s]
1	0.75	10.2	5.0	6.0	12.6	1.5	200
2	1.2	5.1	10	6.3	11.2	1.6	180
3	1.5	10.2	5.0	18	1.4	4.5	21
4	1.5	15.6	1.5	27	0.6	6.9	9.4
5	2.0	10.2	5.0	28.5	0.5	7.1	8.7
6	2.0	15.6	1.5	43.6	0.25	10.9	3.7

Table 9.2: Peak heat fluxes and time for tile surface temperature to reach 1200 C, as a function of plasma current, heating power, and flux expansion. P_{inj}=10.2 MW corresponds to six beam injecting at 80 kV, while 15.6 MW corresponds to six beams injecting at 100 kV. More information on these scenarios can be found in Ref. [19].

Case 1 in the table shows the expected tile heating at I_P=0.75 MA and P_{inj}=10.2 MW, parameters which should be typical of 100% non-inductive operation for 5 second pulses. For these discharge parameters with f_{exp}=15 and f_{div}=0.4, tile heating and thermal stresses will limit the pulse to between 4 and 5 seconds. However, modest increases in the divertor radiation or flux expansion will remedy this problem. Comparatively low input power scenarios at B_T=0.75 T have also been identified that can potentially run for 10 s; case 2 of the table shows that these will require some modest reduction in the heat flux compared to the base parameters. However, the lowest collisionalities are expected for I_P>=1.5 MA, for which scenarios are listed in the final four rows of the table. With f_{div}=0.4 and f_{exp}=15, rapid tile surface overheating and thermal stress accumulations is expected to occur within the duration of the heating pulse for either heating power considered. Note that some expressions for the SOL width scaling have a weaker dependence on I_P than what is used here, with exponents in the range of -1.3 to -1.2. Using this exponent certainly lengthens the time to T_{max} in table 9.2, but does not move it beyond the duration of the heating pulse in cases 3 through 6.

NSTX research has identified two means of mitigating this problem, and these are indicated in the final two columns of Table 9.2. The first is to increase the flux expansion dramatically, using the snowflake divertor. Candidate snowflake divertors in NSTX-Upgrade have flux expansions of 60 to 80; a conservative value of 60 is chosen for the table. The second mitigation strategy is to radiate the power in the divertor volume, before it can reach the divertor surface. This is captured in the above table by reducing f_{div} to 0.1. It can be seen that either of these techniques can reduce the peak heat flux such that the tile heating is not an issue for the duration of the heating pulse in all scenarios but one: the I_P=2.0 MW, P_{inj}=10.2

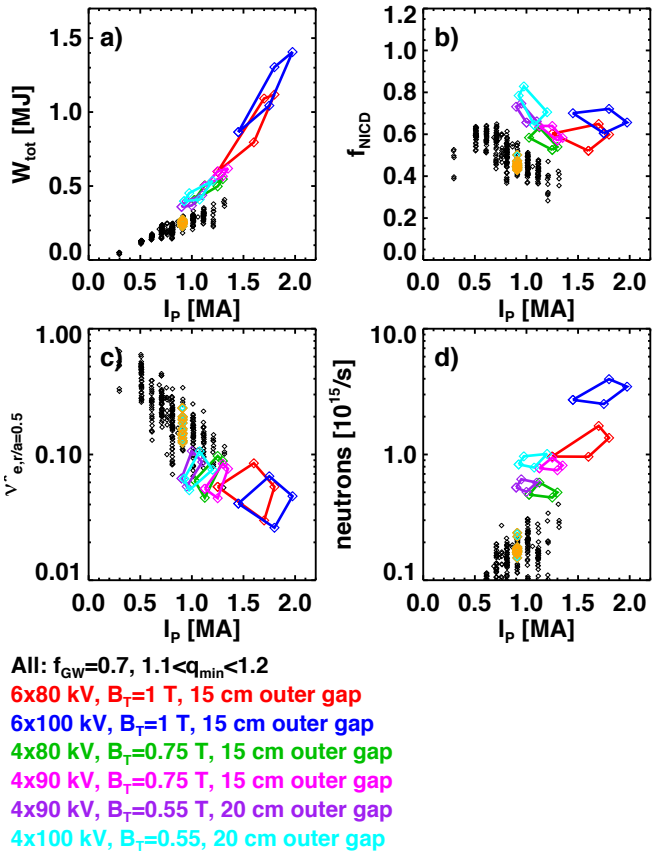

Fig. 9.6: Performance characteristics of NSTX-U scenarios that are predicted to relax to q_{min}>1.1. All NSTX-U simulations are for fully relaxed profiles, and have f_{GW}=0.7.

MW case will likely require a combination of both flux expansion and increased divertor radiation to achieve the desired pulse length with acceptable heat fluxes. Research in NSTX has shown that this exact combination of effects is common when a snowflake divertor is formed in NSTX [14,15].

The details of the NSTX-U strategy for heat flux mitigation are described in the Boundary Physics (BP) Research chapter, and section 9.2.2 of this chapter. Briefly, the development of the physics basis for these two control techniques will be part of the BP research program. ASC research on magnetic control of the snowflake divertor will begin in the first year of the research program, with a goal of providing a "standard" control algorithm by the end of the 2nd year. Development of the measurements and actuators for radiative divertor control will occur in the first two years of research in the BP TSG, and closed loop control experiments will begin in the 3rd or 4th year of the research program.

With this background, the plan for developing long-pulse partial-inductive scenarios is as follows. As discussed in Section 10.7, he first year of NSTX operations is projected to have toroidal fields limited to B_T~0.75T. Under the constraint that the relaxed q_{min} should be greater than 1.1, scenarios with this toroidal field are predicted to be limited to $1.0 < I_P$ [MA]< 1.3 at P_{inj}=6.8 MW, and $1.1 < I_P$ [MA]< 1.35 at P_{inj}=8.4 MW, where the range depends on the confinement assumptions used. Fig. 9.6 shows that these fully relaxed scenarios, indicated in magenta and green, should be able to exceed both the neutron emission and stored energy achieved transiently in NSTX. These relaxed $q_{min}>1$ scenarios at B_T=0.75 T are also not expected to present a thermal challenge to the divertor. The q-profile evolution in these discharges will be used to validate, or drive improvements in, the TRANSP simulations of NSTX-U scenarios.

Experiments will also increase the current towards the 1.5 MA administrative limit planned for the first year, anticipating that this will likely result in q_{min} falling beneath unity. The current redistribution time for these scenarios is expected in to be in the range of 0.5 seconds, so discharges of duration ~$3\tau_{CR}$=1.5 s will be attempted. This time is comparable to the maximum allowed duration due to tile heating in cases 2 & 3 of Table #1, and should allow an early experimental assessment of the thermal heat loading under real divertor conditions.

It is anticipated that full B_T=1.0 T operation with reduced field duration will be allowed in the 2nd year of operations. For relaxed $q_{min}>1.1$ with B_T=1.0 T, TRANSP simulations predict the current levels in Table 9.3 as a function of heating power and Greenwald fraction, with the range again determined by confinement variations. Two of the f_{GW}=0.7 operating points from this table are illustrated in blue and red in Fig. 9.6. These scenarios are anticipated to achieve stored energies in excess of 1 MJ, with neutron flux up to 10 times greater than achieved in NSTX. Experimental time will be spent in the second year accessing these relaxed $q_{min}>1$ scenarios at

B_T=1.0 T. However, the final column of the table shows that the without heat flux mitigation, these scenarios will be limited to short pulse. If snowflake divertors, either pre-programmed or in closed-loop control, are available, they will be used to extend the pulse length. Additionally, the rather high density in these scenarios, chosen to assist in elevating q_{min}, may help raise the divertor radiation fraction and reduce f_{div} compared to the assumption in Table 9.3. Research in the second year will also attempt to extent the B_T=0.75 T scenarios to the full 5 second duration of the heating pulse.

P_{inj} [MW]	Heating Pulse Duration [s]	f_{GW}	Plasma Current Range [MA]	τ_{CR} [s]	Time to T_{max}=1200 C, for middle of I_P range [s]
10.2	5.0	0.7	$1.3<I_P<1.8$	0.45-0.8	1.2
10.2	5.0	1.0	$1.5<I_P<2.0$	0.4-0.7	0.8
12.6	3.0	0.7	$1.4<I_P<1.9$	0.5-0.85	0.65
15.6	1.5	0.7	$1.5<I_P<2.0$	0.6-0.9	0.35

Table 9.3: Current levels and other parameters for relaxed q_{min}>1.1 operations in NSTX-U, for B_T=1.0 T. The tile temperature calculation is based on f_{div}=0.4 and f_{exp}=15.

Experiments will also begin to explore higher-current and lower density scenarios at B_T=1.0 T that may relax to q_{min}<1.1, but have properties favorable for physics exploration. These include short pulse scenarios at I_P up to 2.0 MA. These scenarios will allow a first exploration of transport, global stability, and divertor physics at high-field and current. Monitoring of IR cameras and divertor thermocouples will be used to avoid excessive divertor heating.

The pace of high-current long-pulse development in the latter years will likely be determined by progress in heat flux and particle control. If divertor heating presents the most significant problem, closed loop control of the snowflake divertor may be given additional emphasis, allowing it to be used in scenarios more quickly. If particle control presents the most serious problem, then the ELM pacing and lithium explorations described in the bulleted list at the beginning of this section will receive highest priority. When the cryo-pump is brought on line between the 2nd and 3rd year of operations, it will immediately be used to assist in regulating the density. The ultimate goal for this development will be to form B_T=1.0 T, I_P=2.0 MA discharges that are sustained for 5.0 seconds.

9.2.1.2.2: Research Plans by Year

The time-scale for development of high-current, partial inductive scenarios is summarized as follows:

Year 1 of operations (2015):

- Begin studies of current ramp-up optimization with reduced fueling, including required error field reduction studies.
- Develop short pulses scenarios at B_T=0.75 T and I_P up to 1.5 MA, for studying confinement and divertor physics.
- Extend the discharge durations at B_T=0.75 T and I_P~1.1 MA to the full 5 second pulse duration, using both boron and lithium PFC conditioning.

Year 2 of operations (2016):

- Develop short-pulse scenarios at B_T=1.0 T and I_P up to 2.0 MA, for studying confinement and divertor physics.
- Extend the pulse length at B_T=1.0 T and I_P~1.5 MA to the limits provided by power handling consideration.

Year 3-4 of operations (2017-2018):

- Begin the integration of divertor control techniques, in order to extend the pulse length (see Section 9.2.2.2)
- Establish maximum pulse duration at B_T=1.0T, I_P=2.0 MA, using full complement of current drive and heat flux reduction tools.

9.2.1.3: RF Heating for Advanced Scenarios

As described in Chapter 7 of this 5 year plan, there is a dedicated development effort for coupling high-harmonic fast wave (HHFW) heating and current drive power to NBI heated H-mode plasmas. The goals of that research are to maximize the heating power coupled to the thermal core plasma, and increase the efficiency of core HHFW current drive. Key issues to be resolved include i) reducing the loss of HHFW power in the SOL [33], and ii) reducing the coupling of HHFW power to energetic fast ions [34] (see Sections 7.2.1.2 and 7.2.1.3). ASC researchers will assist in this development, for instance, with control of the antenna-plasma gap regulation or use of density control techniques.

Pending progress in improving coupling, ASC research will dedicate time to couple HHFW heating and current drive into high-performance scenarios, with two goals: increasing the electron temperature for higher non-inductive fraction, and heating and current drive as part of closed-loop profile control. Ref. [19] showed explicitly the benefits of increasing the electron temperature in these scenarios: the bootstrap current is increased by the simple increase in β_P, while the NBCD is increased through lengthening the fast ion slowing down time. These benefits must be weighed against two potential drawbacks of incorporating HHFW to these scenarios. First, the smaller outer gaps favorable for HHFW coupling result in a decrease in the elongation, which causes the large R_{tan} sources from the new beamline to drive their current closer to the magnetic axis. Secondly, the lower densities that may be required to avoid wave propagation in

the SOL [33] may be incompatible with maintaining elevated q_{min} in relaxed profiles or with reducing the divertor heat fluxes. Ultimately, only experimental exploration can determine if the benefits of additional electron heating can overcome these potential issues. Use of HHFW in control loops will be discussed below.

Finally, under incremental funding, the system for EBW heating and current drive may be available for advanced scenario applications in the later phase of the research program. While the primary use of this system is for heating start-up plasmas to increase their coupling to NB and HHFW heating and current drive (see Chapters 7 and 8 for details), it is also possible that this system could provide substantial heating and current drive during the flat top. Current drive efficiencies of 30-60 kA/MW are predicted, which with an ~70% conversion efficiency, indicate that 20-40 kA could be driven with 1 MW of power. Pending the results of dedicated experiments in the wave heating group described in Section 7.2.2.5, exploration will begin for scenarios that incorporate this tool, likely focusing an EBW heating in the during the present research program.

9.2.1.4: Coupling to Non-Inductive Startup and Ramp-Up

As described in Chapter 8, the Solenoid Free Start Up (SFSU) topical science group is researching methods to form and ramp-up the ST plasma current without use of the Ohmic solenoid. This consideration is motivated by the engineering constraint that a full-size solenoid coil capable of ramping the plasma current to full value may be unavailable in next-step STs. Methods under consideration for ST startup in NSTX-U include coaxial helicity injection and plasma gun startup. The subsequent plasma current ramp-up is envisioned to be accomplished by a combination of ECH, HHFW heating, and neutral beam heating and current drive.

This SFSU research on non-inductive ramp-up has many parallels to that described earlier in this section, and ASC researchers will be involved in this development. Particular areas where ASC will contribute include:

- Boundary control at low current, and in the presence of transients, can be challenging. ASC activities will support control of the plasma boundary during non-inductive ramp-up.
- Controlling the density evolution during the current ramp will be critical for controlling the current and pressure profile evolution. The density control tools developed by ASC and BP TSGs will thus be important.
- The modeling of neutral beam current ramp-up has many similarities to modeling the flat-top scenarios, and the ASC and SFSU groups will continue to work together on these modeling tasks. See further discussion in section 9.2.4.3.

The ASC and SFSU research programs will be joined in the later years of this research program. In particular, fully non-inductive flat-top scenarios will be developed for coupling to non-inductive ramp-up, while the ramp-up scenarios will be tailored for coupling to the flat-top. Dedicated experiments will then be conducted to produce discharges with little or no solenoid induction used from breakdown through the end of flat-top as described in Thrust 2 of Chapter 8.

9.2.1.5: Impact of High-Z PFC Conversion on Scenario Development

As described in section 5.3, the base program places high-Z materials in the outboard divertors (see Figure 5.3.1). These locations have been chosen so that the high heat flux regions for high triangularity plasmas remain graphite. Hence, the high-Z upgrades envisioned in the base program should have minimal impact on the scenario development described here.

With incremental funding, the high-Z coverage would be increased more rapidly. In particular, the tiles on the center stack and passive plates would be converted to high-Z materials, as well as the full lower outer divertor and a portion of the upper outer divertor. However, the inner divertor horizontal and vertical divertor targets would remain graphite through this 5 year research program, mitigating some of the risk to high performance scenario development. Under this incremental research program, the development of radiative divertor control (9.2.2.3.2) will be made a high priority for those additional resources. Furthermore, it may be necessary to accelerate the research in safe discharge shutdown techniques. Finally, the use of HHFW in these scenarios may become a higher priority, if it is demonstrated to be a useful tool for controlling the core high-Z impurity content.

9.2.2 Thrust 2: Axisymmetric Control Development

9.2.2.1: Overview of Control Development

As described in 9.1.2.2, axisymmetric control is a critical topic reaching across all areas of tokamak operations and physics. In this section, research on measurements, control loops, and actuators enabling closed loop control are described. NSTX-U research in this area will focus on four broad area: boundary and position control, divertor heat flux control, control of the safety factor and rotation profiles, and particle inventory control.

These control tasks will be executed through the NSTX implementation [35, 36] of the General Atomics Plasma Control System (PCS) [37,38]. At present, the gas injection systems, TF, PF, OH, and RWM coils, and neutral beams [39] are all available to this system as actuators. Present input data include the coil currents, vessel pressure, and extensive magnetic measurements. The

inclusion of additional diagnostic data allowing the execution of the research plan is described below.

For reference, the four sub-topics in Thrust 2 are as follows:

- Advanced boundary and position control (Section 9.2.2.2).
- Control of the divertor magnetic geometry and radiation (Section 9.2.2.3).
- Control of the current and rotation profiles (Section 9.2.2.4).
- Control of the plasma fueling and density (Section 9.2.2.5).

Control of n>0 MHD modes, as manifest in techniques such as resistive wall mode control or error field correction, are described in Chapter 2.

9.2.2.2: Advanced Boundary and Position Control

Control of the plasma boundary is critical for maintaining the high-performance plasma state. Slow boundary control is required in order to maintain high boundary elongation and prevent any of the plasma-wall gaps from becoming too small; note that this problem may be more severe in an ST, where there will likely not be any inboard PF coils to control the inner gap. Fast control is required to stabilize the n=0 vertical mode. This section describes NSTX-U research plans in the area of boundary and position control.

9.2.2.2.1: Realtime Equilibrium Reconstruction and Boundary Control

In order to begin physics operations in NSTX-U, the realtime Grad-Shafranov solver rtEFIT [40] will be upgraded for the new geometry and PF coils of the device. Following that, a reoptimization/retuning of the shape control algorithm is necessary for reliable plasma operations. The boundary control task will produce a Single-Input-Single-Output (SISO) shape controller that connects each of the PF coils to a single, mostly independent, control task such as the outer-gap control, strike point radius control, etc. This development time, as part of device commissioning will restore the ISOFLUX gap control capabilities [40,41] that were used routinely in NSTX. Furthermore, retuning of the strike-point and X-point controllers will be done as necessary, using the relay-feedback control techniques developed for NSTX [42,43].

The underlying tool for boundary control in NSTX-U is realtime equilibrium reconstruction. The previous real time EFIT reconstructions in NSTX used 33x33 grid spacing. The accuracy of this reconstruction is insufficient for many of the tasks in NSTX-U such as snowflake divertor calculations. The primary reason for the course grid has been the computational load on the real-time computers. However, with the upgrade to the computer hardware and software described in Section 10.3.3.4, NSTX-U will have substantially greater realtime computing power, allowing higher resolution 65x65 grid reconstructions to be tested and implemented for NSTX-U.

A second improvement to the rtEFIT reconstructions will be made via improvements to the constraint set. In NSTX, only magnetic measurements were used to reconstruct the plasma state; this will be the initial state when operations resume in NSTX-U. Research during the 5-year period will include the development of real-time kinetic measurements, such as MSE and MPTS. When such measurements become available, including them as constraints to the rtEFIT reconstruction will be high priority. For instance, the rtMSE diagnostic will provide a strong constraint on the q-profile, for use in q-profile control development described in Section 9.2.2.4.1. This diagnostic will also provide a strong constraint on the magnetic axis location, helping to constrain β_N via knowledge of the Shafranov shift. The realtime MPTS data can also help resolve the Shafranov shift correctly, as well as help resolve the plasma outer boundary more accurately. The planned availability of real-time MSE is late in the first year of operations, or possibly during the second year, and work on rtEFIT reconstruction with MSE will start as soon as that data is available. Real-time MPTS may be available during the final years of the 5 year plan, and will be used as either part of an isotherm or loose isobar constraint [44].

SISO boundary control will be used for initial NSTX-U operations, based on its comparatively fast implementation time and proven capability in the base NSTX scenario operations. However, this approach may not be sufficient to reach the full operation capabilities of NSTX-U. For instance, due to the small radius of the center columns, NSTX-U and future ST devices will not have PF coils on the inner wall to specifically control the inner gap. This can result in uncontrolled inner gap motion when other shape parameters are modified or the plasma profiles change. Furthermore, the new snowflake divertor will need a new complex control for the divertor region PF coils in both upper and lower divertor regions (see Section 9.2.2.3.1) which will interact with the control processes for the other PF coils. If these or similar phenomenon result in operational problems, ASC researchers will begin a program in multi-input, multi-output shape control development. In this case, this task involves coupling the voltage requests for the PF coils to more distant shape control points. For instance, the coils that control the divertor geometry will also be tasked with some control of the inner gap. The control code exists for this in the present ISOFLUX shape control, but has not been exercised. Relay-feedback optimization will be used to develop the optimal control gains.

As the facility develops, continued development of shape control algorithms will likely be required. For instance, the NSTX-U plan calls for a cyro-pump to be installed after the second year of operation. The pumping provided by this system is extremely sensitive to the strike point location, and special strike-point control development may be required. Furthermore, the PF-2 coil may be upgraded to bipolar capability. This would open up additional possibilities for control of the bottom gap in high-triangularity and elongation scenarios, and development tasks to exploit this capability would be executed.

9.2.2.2.2: Vertical Position Control

Vertical position control may restrict the operating space available to the NSTX-U physics program. An example of this can be seen if Fig. 9.7, taken from the high-A and κ experiment conducted during the short 2011 run campaign; one of the discharges is typical of NSTX at κ~2.5 and A=1.45, while the other pushes κ towards 2.9 and the aspect ratio to 1.7. In the high-A cases, transient increases in l_i resulted in the control system reducing the PF-3 currents, in an effort to maintain the plasma elongation. As the PF-3 coil currents become smaller, the stabilizing field index was reduced, eventually leading to a vertical displacement event and disruption. Reducing the requested elongation would have resulted in an increase in the PF-3 current, and restoration of vertical stability.

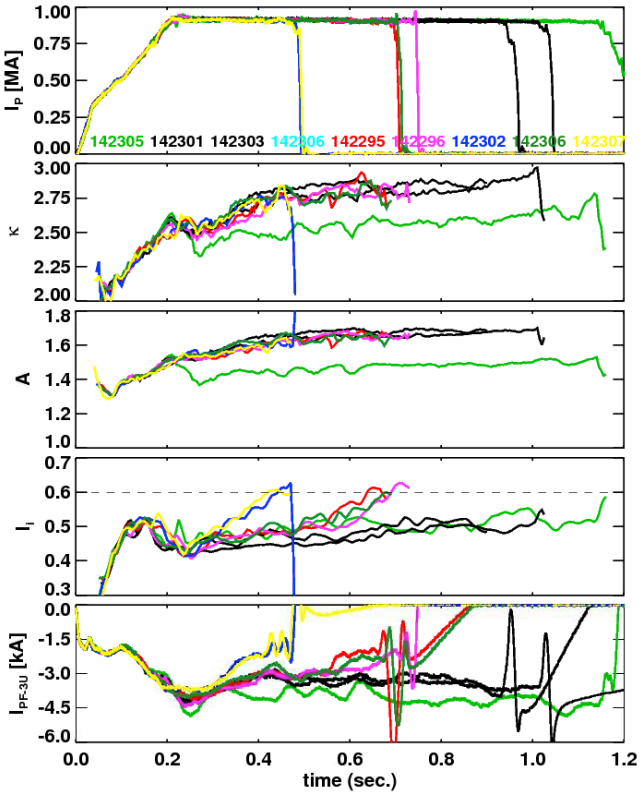

Fig 9.7: Loss of vertical position control when the internal inductance reached a threshold value in higher aspect ratio discharges.

While operation with bad field curvature will never be feasible and certain portions of κ-l_i space will not be accessible, this result underscores the importance of optimizing the active vertical stability control. The following steps have been implemented to potentially improve the vertical position control of NSTX-U plasmas:

- Added additional poloidal flux loops to the vertical position observer. This should provide a more accurate and less noisy measurement of the plasma position and velocity for use in feedback control.
- Added PCS code to use the n=0 radial field from the RWM coils for feedback control of the vertical position. The field from these coils is significantly smaller than from the large PF-3 coils, but this system has the advantage of a more rapid power supply response, with less conducting structure between the coils and the plasma.
- Improved the digital communication links between the realtime computer and the large radial field coils (the PF-3s). This will result in a reduction in the latency of the position control.

- Moved the PCS code for vertical position control to a new PCS "category". This will allow more rapid addition of new vertical control algorithms, and will provide the capability to easily add additional PF coils to the vertical control loop should that prove desirable.

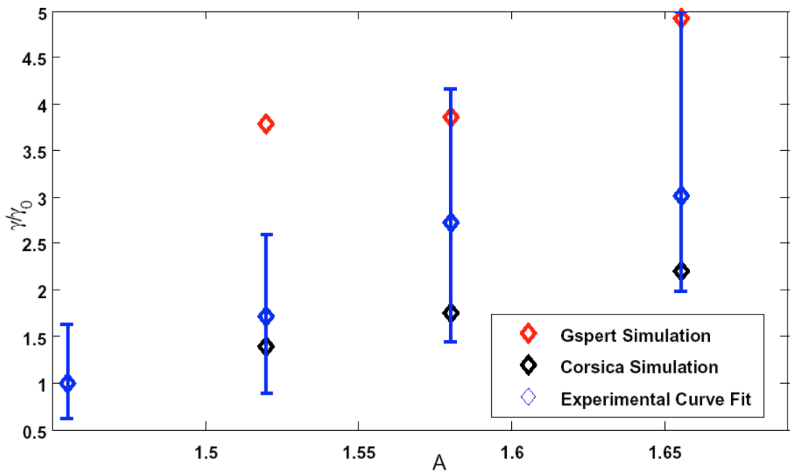

Fig 9.8. Change in γ versus A for Corsica and Gspert simulations, and experimental data (#141639-141642)

It is expected that the improvements noted above will improve control of the vertical stability with the regular constant coefficient Proportional-Derivative (PD) control scheme, as has been used in NSTX and other many major tokamaks such as DIII-D, JET and EAST [45]. However, a plan has been formulated to improve the vertical control algorithm in case the PD control proves inadequate. There are usually two sources of poor vertical control performance. The first is the actuator (PF coil) saturation, while the second is measurement noise, potentially due to effects such as ELMs and n=1 RWM/locked-mode pickup. If the main issue is assessed to be actuator saturation, a higher-level control implementation such as an anti-windup scheme will increase the control stability by avoiding reaching the voltage/current limits of the coils. An example of anti-windup vertical position control for a tokamak is shown in [46]. Similarly, if the main control issue is measurement noise, a more sophisticated algorithm that is robust to noise, such as a non-linear adaptive optimum control, will be developed [47].

Finally, the infrastructure for real-time vertical stability calculations will be included in the PCS during the later years of the research program. This will enable real-time adjustment to the vertical stability control during the shot. One potential method for attaining this information is to measure vertical growth rates perturbatively using relay-feedback algorithms (see for example [48] and reference within). In this method, the vertical control is modified for a short amount of time. The control response induces the system to oscillate at its unique frequency and amplitude, which can be used to find the vertical stability of the system.

Alternatively, the vertical stability can be computed using stability codes. Fig. 9.8 compares numerical simulations to experimental data from aspect ratio scans, where the vertical position

control was frozen and the plasma allowed to drift [49]. The n=0 growth rates were calculated with Gspert [50], a non-rigid plasma response model based on the linearized Grad-Shafranov equation, and CORSICA [51], a free-boundary equilibrium and transport code. The simulations are in reasonable agreement with the experimental results. Thus, the simulation results, if available in realtime, could be used as a proxy for measurements of the vertical stability.

Research in the later years of the plan will assess whether a real-time version of Gspert code should be included in the PCS, or whether a perturbative-like stability analysis will be required. This information would be used to change the vertical position control law, or trigger a loss of control alarm (see Section 9.2.3.1.3).

9.2.2.2.3: Research Plans by Year

The time-scale for these boundary and vertical position control activities are summarized as follows:

Year 1 of operations (2015):

- Retune the PD vertical control algorithm with improved measurement and actuator capabilities. Assess the vertical stability.
- Restore the SISO boundary and strike point control capabilities in NSTX-U.
- Begin implementation of the higher resolution (65 x 65) version of rtEFIT.
- Begin implementation of the real-time MSE constrained version of rtEFIT.

In the case that the vertical control is not satisfactory, make improvements during years 1 and 2:

- Assess the conditions under which the vertical control system fails. Model the vertical motion of the plasma and disturbances such as ELMs.
- If the main issue is the actuator saturation: Implement a new anti-windup vertical control algorithm.
- If the main issue is disturbances in the measurements: Implement a new noise filter for the vertical motion observer that takes into account ELMs and other disturbances.

Years 2 of operations (2016):

- Test and implement higher resolution (65 x 65) version of rtEFIT.
- Based on diagnostic availability, implement and test the real-time MSE constrained version of rtEFIT.
- Assess strike-point control capabilities and make necessary improvements in anticipation of cryo-pump operation.

Years 3-4 of operations (2017-2018):

- Implement real-time vertical stability calculations for improved vertical feedback and loss of control detection.
- Test and implement improved rtEFIT using additional non-magnetic measurements as constraints (for instance, realtime MPTS)
- If it appears necessary, begin the implementation of MIMO shape control.

9.2.2.3: Closed Loop Control of Divertor Magnetic Geometry and Radiation

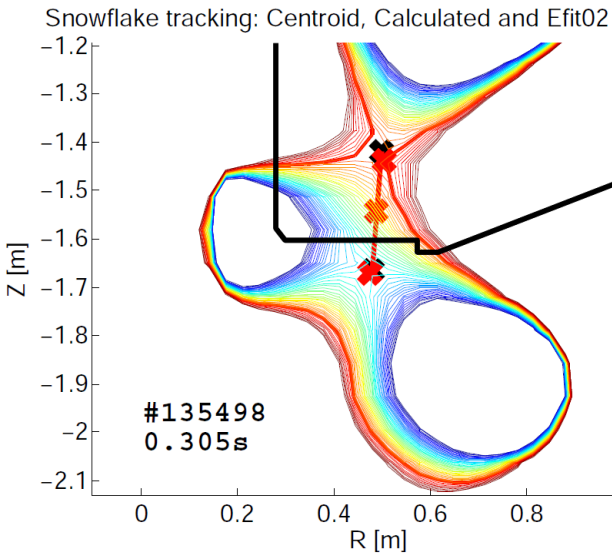

Fig. 9.9. Snowflake tracking for NSTX: Red crosses are the algorithm computed snowflake centroid and the X-points; Black crosses are the calculated real X-points.

As noted in the context of table 9.2, the heat flux in NSTX-U is projected to be quite large, easily exceeding 10 MW/m^2 if it is not actively mitigated. The unregulated heating of the divertor surface will rapidly result in the surface temperature exceeding the 1200° C sublimation limit of carbon. This section describes the NSTX-U strategies for closed loop control of divertor heat fluxes: magnetic control of the snowflake divertor, and feedback control of the divertor radiation via gas puffing

9.2.2.3.1: Snowflake Divertor Control

The snowflake divertor (SFD) is formed when a second divertor coil is used to introduce an additional X-point in the vicinity of the "primary" X-point; see discussion in section 4.2.2. The SFD has resulted in very large divertor poloidal flux expansions, which as a geometric effect directly reduces the heat flux. Interestingly, NSTX divertor heat fluxes have been reduced even beyond that expected from geometric effect, due to inducement of outer-strikepoint detachment with the SFD [14]. Hence, the SFD is a key tool for reducing the divertor heat flux. However, magnetic control of the SFD, required to maintain the geometry against changes in plasma profiles or the current in the other poloidal field coils, has not yet been attempted.

The implementation of SFD control in NSTX-U will utilize two steps:

- Realtime tracking of simultaneous X-point will be implemented, in collaboration with GA and LLNL.
- Additional terms will be added to the divertor coil feedback loops, to do snowflake divertor control.

The realtime tracking of multiple X-points will be accomplished with an algorithm that uses a local expansion of the Grad-Shafranov equation [52,53].

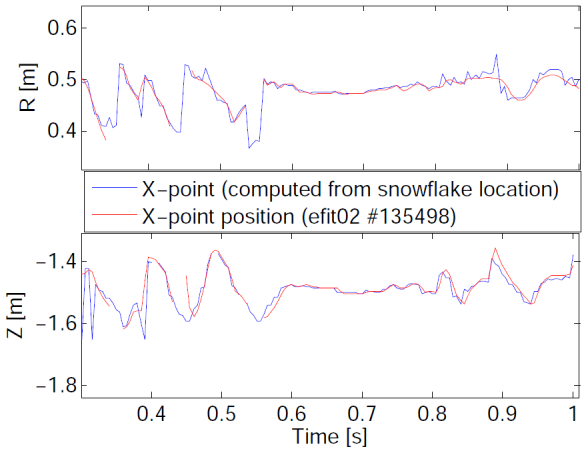

Fig. 9.10: Comparison of the X-point position computed from the tracking algorithm and the EFIT02 calculations.

$$(R+x)\frac{\partial}{\partial x}\left(\frac{1}{R+x}\frac{\partial \Psi}{\partial x}\right)+\frac{\partial^2 \Psi}{\partial z^2}=0$$

Keeping the 3rd order terms allows the dual magnetic nulls to be found given the values of the poloidal flux at three given sample points. Note that this is a one-step algorithm, which does not require any iteration. An offline version of this algorithm has been implemented and tested against the EFIT calculations as shown in Fig. 9.9. The algorithm is able to find the snowflake centroid and approximate X-point locations with good accuracy. Tracking results for the algorithm for a full shot is shown in Fig.9.10. The algorithm robustly finds the X-points at every time point without computational instabilities, which is required for essential real-time computation. A PCS version of this code will be implemented using the equilibrium reconstructions from rtEFIT to provide the poloidal flux map.

Once the X-point locations have been determined, they must be used for feedback control: this will be accomplished within the existing NSTX implementation [41] of the ISOFLUX shape control algorithm [40] as follows. The code that computed the PF coil voltages will be upgraded to contain a new term, listed second in the standard formula for the coil voltage request:

$$V_{PF} = M_{mat} PID(E_{seg}) + X_{mat} PID(E_{snow})$$

Here PID is the standard proportional, integral, and derivative error operator. E_{seg} is a column vector that contains the segment flux errors as computed by rtEFIT, while M_{mat} is a matrix which maps the elements of PID(E_{seg}) to the various coil voltage requests; both of these presently exist in the ISOFLUX control algorithm. E_{snow} is a new column vector of SFD related geometric quantities. These could include the radius and height of the primary X-point, the distance between the primary and secondary X-points, and the angle of the line connecting these X-

points. The matrix X_{mat} maps the result of the PID operator on the SFD errors to the PF coil voltage requests. In this way, closed loop control of the SFD can be completed.

The parameters to be used in these feedback loops will be determined in two steps. First, free-boundary equilibrium codes like ISOLVER will be used to determine initial guesses for the proportional control gains. Then relay-feedback techniques, as implemented for single X-point divertor control and described in Ref. [43], will be used to tune the gains for optimal control fidelity.

It is anticipated that SFD control development will begin in the first year of NSTX-U operations, with realtime tracking of the X-points and modifications to the ISOFLUX control algorithm taking place. The upper and lower PF-1A, PF-1C, and PF-2 coils will be used for control in this initial development. More advanced tuning of the algorithm will be completed in the second year of operations. A key issue to be addressed in this development is the maintenance of the up-down magnetic balance (dr_{sep}) in the presence of 4-X-points, so that the 50% power splitting between the upper and lower divertors is maintained. Experiments will also examine the maintenance of the SFD during the OH flux swing. Some calculations [11] suggest that the PF-1B coil will be necessary for precise SFD control over the full range of OH coil currents, and a decision on the powering of this coil will be made after this campaign. Final control development, including possible tuning with the additional PF-1B coils, will be complete in the third year, and use of this control in scenario development will begin at that time.

9.2.2.3.2: Radiative Divertor Control

Beyond active control of the divertor geometry, scenario and control research will assess direct control of divertor radiation via feedback control of impurity gas injections. This effort, in conjunction with the Boundary Physics (BP) research group, will be completed in two steps.

During the first two year of operations, a focused effort will be made in the BP group to determine the best realtime measurements for actuating the impurity gas flow. As described in Ref. [54], measurement options that have been identified include:

- Radiated power measurements, for instance, using AXUV diodes.
- The divertor neutral pressure, measured, for instance, by Penning gauges.
- Recombination radiation from Balmer or Paschen series deuterium lines, measured by an imaging EUV spectrometer.
- Surface temperature measurements from infrared thermography.
- Thermoelectric SOL currents.

These options will be examined for sensitivity, reliability, and ease of implementation in realtime, and dedicated efforts to bring the signals into the PCS will begin in the 2nd and 3rd years.

Simultaneously, control of appropriate gas injectors by PCS will be implemented. It is envisioned that at least two upper and two lower divertor gas injectors will be utilized, at first for open loop experiments in the BP TSG.

These development tasks can be brought together by the fourth year of NSTX-U operations. Initial closed loop control experiments will then be executed. A first step will be simple PID control, for instance, with the voltage on the gas injectors given by V=PID(E), with E the error between the reference and measured diagnostic signal. Steady-state control of the divertor radiation and reduction of the divertor heat flux should be demonstrated, for discharges much longer than the current relaxation time, and without degradation of the H-mode pedestal. If needed, and time permitting, realtime monitors of the pedestal performance will then be used to regulate the feedback, in order to prevent over-fueling of the radiating gas.

9.2.2.3.3: Research Plans By Year

The time-scale for these divertor control activities under the base program is summarized below. Under incremental funding, the radiative divertor control experiments can be accelerated by at least a year.

Year 1 of operations (2015):

- Implement realtime X-point tracking and modifications to the shape controller to allow dual X-point control. Make first attempts at snowflake divertor control.

Year 2 of operations (2016):

- Begin development of realtime heat flux or divertor radiation diagnostics.
- Optimize closed-loop control of the snowflake divertor.

Year 3-4 of operations (2017-2018):

- Finish development of realtime heat flux and radiated power diagnostics, and begin development of radiative divertor control.
- Use close-loop control of the snowflake divertor in high-current, high-power, long-pulse scenarios.

Under incremental funding, high priority would be given to accelerating the radiative divertor control development. In particular, realtime measurements associated with this control would be brought into PCS earlier in the research period, and the additional run time would allow this research to be initiated more quickly. This choice of priority supports the plan to convert most of

first wall, and a fraction of the divertors, to high-Z metal by the end of the 5 year plan period given incremental funding.

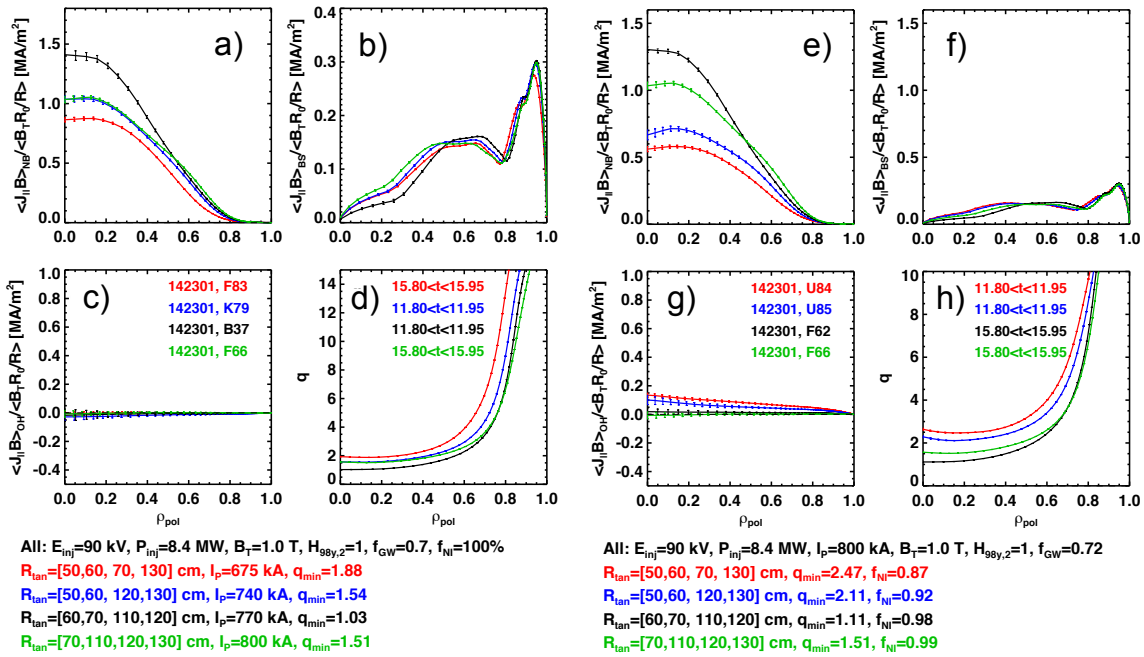

Fig. 9.11: Control of the safety factor profiles (frames d) and h)) by varying the choice of neutral beam sources. The four frames at the left are calculations at constant non-inductive fraction of 100%, while those at the right are at constant current of 800 kA.

9.2.2.4: Profile Control

The shape of the rotation and safety factor profiles can have a profound impact on the performance of the discharge. For instance, increasing the central safety factor can improve the stability of n=1 internal kink/tearing modes, but can also result in an increase in thermal transport. The correct toroidal rotation profile can result in stabilization of the resistive wall mode, while toroidal rotation shear can improve the stability of m/n=2/1 neoclassical magnetic islands. Toroidal rotation is also believed to modify the turbulent transport level through its impact on ExB shear. Hence, controlling these two profiles is critical for optimizing tokamak and ST scenarios.

9.2.2.4.1: Safety-Factor Profile Control

With regard to the safety factor profile, NSTX-U will have a number of important actuators. The impact of the plasma density on q_{min} in scenarios with large non-inductive fractions was already discussed in conjunction with Fig. 9.3, where it was shown that raising the density results in an increase in q_{min}. As shown in Ref. [19], increasing the outer plasma-wall gap increases the

elongation and the effective tangency radius of the neutral beam relative to the magnetic axis, resulting in an increase in the minimum safety factor. However, changes to the outer gap and plasma boundary shape will impact many other features of the discharge. Hence, it is important to consider a third key actuator on q_{min}: the neutral beam source selection.

Fig. 9.11 shows TRANSP calculations of the impact of variations in the beam source selection on the safety factor profile. The set of four plots on the left is done under the constraint of fixed non-inductive fraction of 100%, while the set of four plots on the right has a constant plasma current of 800 kA. The plasma is heated by four 90kV neutral beams in all cases, with a toroidal field of B_T=1.0 T and Greenwald fraction of f_{GW}=0.7. All profiles are fully relaxed, and classical beam physics is assumed.

The left hand plots show that fully relaxed q_{min} can vary between 1.0 and 1.9, and the plasma current can vary from 675 kA to 800 kA, with 100 % non-inductive current drive. The lowest-current, highest-q_{min} case uses the original three NSTX beam sources, with their lower current drive efficiency, as well as the single largest R_{tan} source of the new beamline. This combination of sources results in a slightly less peaked NBCD profile, and less overall NBCD. The lowest-q_{min} case, on the other hand, uses the four sources which produce the most central NBCD: the smaller R_{tan} sources from the new beamline and the larger R_{tan} sources from the old beamline. The highest non-inductive current level comes when using R_{tan}=[70,110,120,130] cm sources, which have the highest current drive efficiency

The right hand set of four plots show a relaxed q_{min} varying between 1.1 and 2.5, for fixed I_P = 800 kA, as the non-inductive fraction varies between 87% and 100%. Once again, the lowest q_{min} comes from using the R_{tan}=[60,70,110,120] cm beams, the first two of which are from the old beamline and the last two of which are from the new beamline, while the highest q_{min} occurs with the R_{tan}=[50,60,70,130] cm sources. The highest non-inductive current fraction comes again when using R_{tan}=[70,110,120,130] cm sources.

Initial experiments on q-control will utilize feed-forward programming to verify that the predicted variations in q_{min} will indeed occur. Experiments in the first year of operations will focus on the cases with fixed plasma current, as in Figs. 9.11e)-h). The relaxed current profiles with different beams injecting will be measured, and then compared to the predictions from classical models such as are in TRANSP; these comparisons will use the measured thermal profiles, so that transport variations can be removed from the studies. The experiments will be conducted at lower densities, where the effects of the different sources may be more profound that in Fig. 9.11, and a higher densities, where the effect may be smaller. As the non-inductive scenarios are better developed in the second and third operational years, the calculations in the left frame documenting q_{min} variations in 100% non-inductive scenarios will be experimentally

tested. These experiments will also provide data for assessing the role of *AE activity on fast ion physics, as described in Sections 9.2.4.2.

In parallel with these actuator validation/development activities, the development of current profile controllers will begin. Two parallel efforts will be required to make these efforts successful: implementation of realtime q-profile measurements, and development of appropriate control algorithms.

The realtime measurements of the q-profile will be implemented as part of the NSTX collaboration with Nova Photonics. Up to 18 channels of pitch-angle data will be available in realtime, spanning from the small-radius side of the magnetic axis to the outboard midplane SOL. It is presently envisioned that the processing of the pitch angle data, requiring very rapid acquisition, will be done on dedicated computers, and only processed pitch angle and status bits provided to the plasma control system. These pitch angle measurements will be used to constrain the rtEFIT reconstructions, providing an accurate realtime measurement of the safety factor profile. It is anticipated that this system will be developed during the 1st year of NSTX-U operations, with calibrated realtime pitch angle data available to PCS during the 2nd year. See section 10.6.3.2 for additional information on this diagnostic system.

The measurements and actuators are connected by control algorithms. These profile control algorithms are under active development and experiments are being conducted on the DIII-D tokamak. One of the aims of this DIII-D participation is to gain insight into the best possible NSTX-U profile control implementation. Based on this experience, the planned profile control for NSTX-U is based on gray box control, which relies on physics based model with experimentally obtained coefficients. These models are simplified and experimentally fitted coefficients are used to develop plasma profile control algorithms. Lehigh University collaborators have already designed and tested some q profile controls based on physics model [55,56]. The evolution of the current profile can be written from Faraday's law as [57]

$$\frac{\partial \psi}{\partial t} = \left(\frac{< \vec{E} \cdot \vec{B} >}{< R^{-2} > f} \right),$$

where f (R, Z) = RB_φ(R, Z) in the cylindrical coordinates, (R, φ, Z). This expression is then expanded to

$$\frac{\partial \psi}{\partial t} = f_1(\hat{\rho}) u_1(t) \frac{1}{\hat{\rho}} \frac{\partial}{\partial \hat{\rho}} \left(\hat{\rho} f_4(\hat{\rho}) \frac{\partial \psi}{\partial \hat{\rho}} \right) + f_2(\hat{\rho}) u_2(t)$$

using experimental obtained data $f_1(\hat{\rho})$, $f_2(\hat{\rho})$ and $f_4(\hat{\rho})$ to obtain a nonlinear diffusion equation with the forcing terms $u_1(t)$ and $u_2(t)$ which are the functions of the control actuators

such as NB and HHFW. In order to find an optimal control, the cost function, which is the sum of the error in iota and control effort,

$$J = \frac{1}{2}\int_0^1 \alpha(\hat{\rho})(\iota^*(\hat{\rho}) - \iota(\hat{\rho},T))^2 d\hat{\rho} + \frac{1}{2}\sum_{i=1}^{3}\gamma_i \int_0^T u_i^2(t)dt$$

is minimized. Extremum-seeking [55] and nonlinear-programming [56] algorithms have been considered for the numerical solution of this optimal minimization problem. Similar gray box control designs will be implemented at NSTX-U PCS for profile control. Note that initial "tuning" of these controllers will be done with TRANSP simulations of the type described above. The controllers can then be refined based on actual experimental data.

Assuming that pitch angle data from rtMSE-constrained rtEFITs are available in the 3rd year of operations, first attempts at combined q_{min} and β_N control will be done. The neutral beams, and potentially the loop voltage, will be the sole actuators for these first studies. Here, the β_N component of the control is likely a loose constraint, needed to prevent the input beam power from becoming too large or too small, both of which will lead to disruption. This combined q_{min} and β_N control will be refined in subsequent years, until it can be a reliable control tool for NSTX-U.

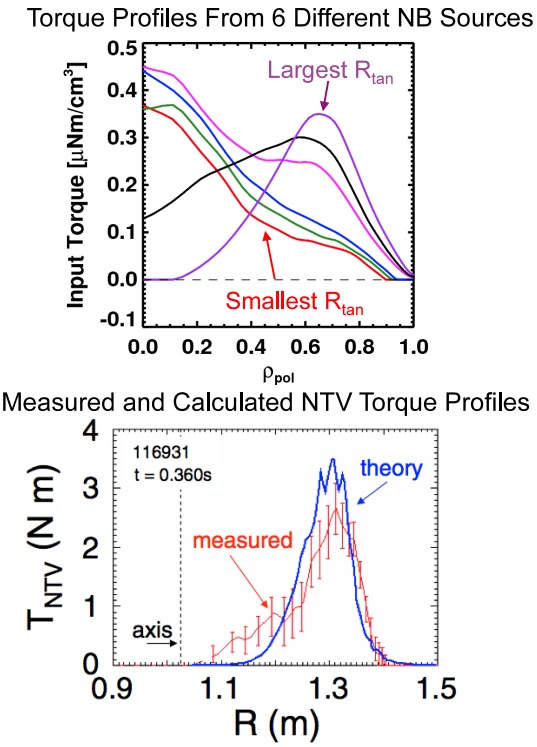

Fig. 9.12: Torque profiles from a) the six NSTX-U neutral beams, and b) applied 3D fields from NTV

In the later years of the plan, additional goals and actuators will be included. For instance, if viable schemes for HHFW heating of H-mode plasmas are developed, then the HHFW system will be included in the control loop. This will allow a heating system with no current drive, increasing the flexibility of the controllers. Research in those later years will also assess the ability to control additional points on the q-profile, instead of q_{min} alone.

The schedule for the implementation of current profile control is indicated in Section 9.2.2.4.4.

9.2.2.4.2: Rotation Profile Control

As noted in the introductory paragraph to this section, the second profile of interest for control is the rotation profile. In this case, the two actuators under consideration are the neutral beams and 3D fields.

Fig. 9.12a) shows the torque profiles for the six NSTX-U neutral beam sources. The innermost three sources, corresponding to the original NSTX beamline, produce centrally peaked torque profiles, and are not expected to have profoundly different impact on the plasma rotation beyond the different scale factors on the profiles; this was indeed the operational experience in NSTX. However, the three new sources have profoundly different torque profiles. The R_{tan}=110 cm waveform remains centrally peaked, but with a "bump" near the mid-radius. The R_{tan}=120 and 130 cm sources are peaked off axis, with the largest R_{tan} source providing minimal on-axis torque.

The second actuator for use in rotation profile control is NTV (neoclassical toroidal viscosity) magnetic braking [58-60] using the EFC/RWM coils. Experiments have shown that the torque profile from the 3D fields tends to be peaked at about the mid-radius, since the torque is proportional to $T_i^{5/2}$ (increasing inwards) and δB^2 (increasing outwards). Numerous experiments have demonstrated that magnetic braking can provide excellent open-loop control of the rotation magnitude [60,61], and it is anticipated it will be an excellent braking actuator in closed loop as well.

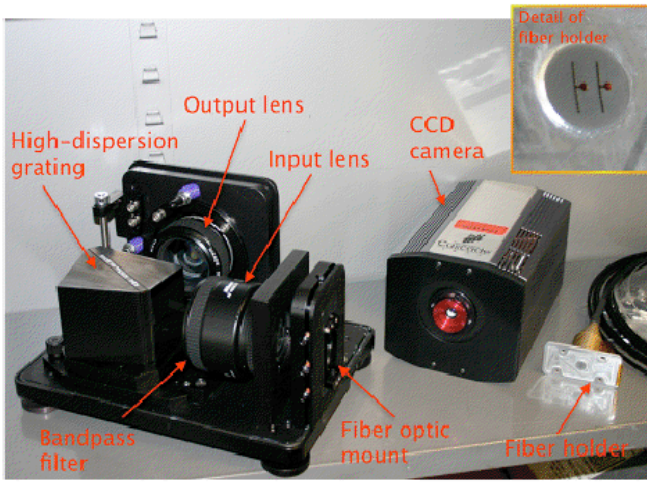

Fig. 9.13 Camera hardware associated with the RTV diagnostic.

As with q_{min} control, once the actuators have been understood, the technical steps required to implement closed loop control include the development of realtime diagnostics and the implementation of control algorithms.

With regard to realtime velocity diagnostics, the RTV system shown in Fig. 9.13 has been designed and implemented [62]. This system utilizes two cameras, each of which monitors two radial locations in the plasma. The four measurements capture the rotation in the plasma core, the plasma edge, and two intermediate locations. These locations were selected to enable an optimal resolution of the rotation profile, given the constraint that only spare fibers from the offline

toroidal CHERS system were available for use. Non-linear fitting routines are used in realtime to compute line shifts, and readout and line fitting from test light sources has been demonstrated at 1 kHz. It is anticipated that this system will be commissioned in the 1st year of NSTX-U operation, for use in control during the 2nd year.

Initial work on the development of model-based rotation control algorithms has been completed [63]. In this work, a reduced toroidal angular plasma momentum equation was obtained by examining the NSTX experimental data, as processed by the TRANSP code. The angular velocity of the plasma, ω, can be described dynamically by the flux surface average of the one-dimensional toroidal momentum equation:

$$\sum_i n_i m_i \left\langle R^2 \right\rangle \frac{\partial \omega}{\partial t} = \left(\frac{\partial V}{\partial \rho} \right)^{-1} \frac{\partial}{\partial \rho} \left[\frac{\partial V}{\partial \rho} \sum_i n_i m_i \chi_\phi \left\langle R^2 (\nabla \rho)^2 \right\rangle \frac{\partial \omega}{\partial \rho} \right] + T_{\mathrm{NBI}} + T_{\mathrm{NTV}}$$

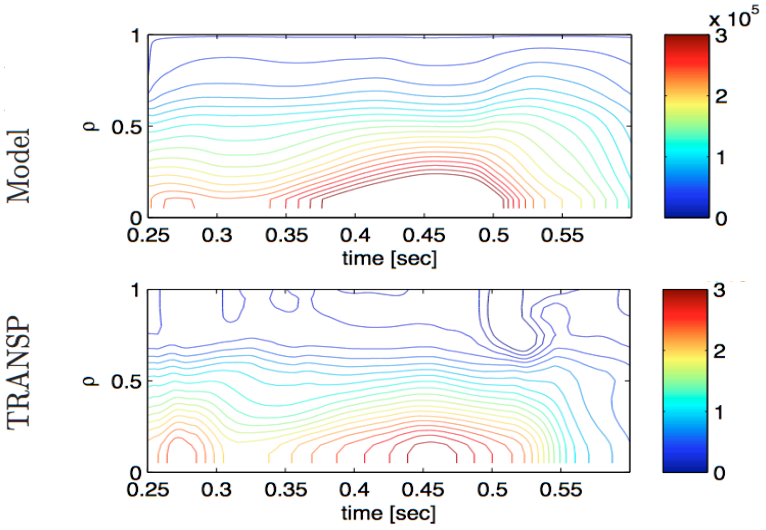

Fig. 9.14: Contour plots showing a comparison of that rotational frequency ω [rad/sec] from the simplified model and TRANSP data for shot 128020.

In this exercise, the torque from neutral beams was modeled as a Gaussian spatial distribution with a first order time constant in the temporal domain and the NTV torque was modeled as a linear function of rotation with a modified Gamma function in the spatial distribution with a first order time constant in temporal domain. The simplified rotation evolution model was validated with the NSTX experimental data as shown in Fig. 9.14, using the experimental χ_ϕ profile data. The qualitative behavior of the rotation is captured with this model and indicates that the actuator models are sufficient for model development.

Based on the actuator and the rotation evolution models new algorithms to control the rotation profile were developed. A time-dependent LQR (Linear Quadratic Regulator) control algorithm was designed using the Neutral Beams and the 3D coils as actuators. Fig. 9.15 shows a simulation of the normalized rotation profile under this control when a broad 10% average increase in rotation profile is requested. It is predicted that with the new control, regulation of the

rotation profile within the fully controllable phase space capabilities of the actuators will be possible.

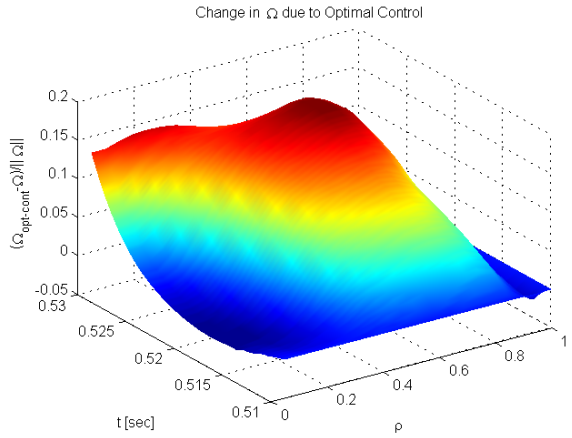

Fig. 9.15: Simulation of the normalized rotational frequency profile change of the plasma under the LQR control.

Assuming that realtime camera data is available in the 2nd year of NSTX-U operations, rotation control development will begin at that time. Work in the 2nd year will begin with combined $F_{T,0}$ and β_N control, using the NBs and 3D fields as actuators (here $F_{T,0}$ denotes the central rotation frequency). Work in the third and fourth years will extend the control to additional spatial points, for instance, the mid-radius, and potentially a point near the edge of the plasma. Furthermore, research with the MS group will begin, where rotation control is used as a component in integrated disruption avoidance studies (See section 2.2.3.1 for additional information on those studies). If schemes with reliable HHFW heating in H-mode can be identified, then HHFW will be used to provide heating without torque input in these control loops.

Finally, while q_{min} and F_T control will be implemented as somewhat separate research lines initially, the long-term goal of the research is to use them simultaneously. In the latter years of the proposal, combined control of the rotation profile, q_{min}, and β_N will be assessed and implemented if it appears feasible. Reliable schemes for HHFW heating will likely be a very beneficial for these control scenarios, in order to provide heating without torque or direct current drive.

9.2.2.4.3: Collaborations in Profile Control

Recently, PPPL has been expanding collaborations within the control engineering community. Princeton University Mechanical and Aerospace Department collaboration under the leadership of Prof. Clarence Rowley have been working on the producing reduced order models specifically useful for model-based control development. This collaboration already produced valuable solutions in strike point and boundary control. Longer-term plans are to develop integrated controllers, which can address multiple objectives (e.g., vertical mode stabilization, strike point control, shape control, and rotation control) within a single control design.

The new collaboration with Lehigh University under the leadership of Prof. Eugenio Schuster began in 2013. The aim of this work will be to study and understand the current profile dynamics

for NSTX-U, to develop current profile control algorithms that enable the efficient and optimal use of the actuators using modern model-based control approaches, and in this way to further the scientific mission of the NSTX-U. The main task of this collaboration is the development of validated reduced control-oriented dynamic models of the NSTX-U plasma current profile evolution, the diagnostic measurements, and the effect of the actuators on the plasma. Then, with these models, the collaborators will development real-time current-profile control algorithms based on the developed control-oriented dynamic models. These control algorithms will be tested and tuned using TRANSP simulations.

9.2.2.4.4: Research Plans by Year

The time-scale for these profile control activities under the base budget is as follows. Note that because the primary actuators (the neutral beams, 3D field coils) are already in the baseline plan, the rtV_ϕ diagnostic is already well along in development, and the rtMSE system is a funded collaborator diagnostic, it appears that the primary benefit of incremental funding is increased run-time, allowing the development to be completed more rapidly.

Year proceeding operations (2014):

- Do initial control designs with Princeton University and Lehigh collaborators.
- Do test stand development of the realtime MSE diagnostic.

Year 1 of operations (2015):

- Perform initial validation of q_{min} control via changes in the beam sources in partial inductive scenarios.
- Implement realtime MSE and V_ϕ diagnostics. Incorporate MSE measurements into rtEFIT.

Year 2 of operations (2016):

- Begin development of combined β_N and $F_{T,0}$ control
- Finish validation of q_{min} control via beam source selection in partial inductive scenarios, and begin validation in 100% non-inductive scenarios.

Year 3-4 of operations (2017-2018):

- Begin joint research with the MS group on integrated disruption avoidance, using rotation control as an actuator.
- Add additional spatial points to the rotation controller, for instance control of the central and edge rotation in addition to β_N.
- Begin development of combined β_N and q_{min} control, expanding to additional points on the profile as appears feasible.
- If feasible, incorporate HHFW into the profile control algorithm, for improved decoupling between heating and momentum or torque actuators.

9.2.2.5: Deuterium Inventory Control

The phrase “density control” has been used elsewhere in this plan to indicate the achievement of non-evolving plasma density, typically via the pumping provided by a new cryo-pump. This section, however, addresses closed loop control of the deuterium inventory in terms of the measurements, actuators, and control loops, to be developed in collaboration with the BP TSG as described in Chapter 4. When impurity control techniques, such as ELM pacing or the development of small-ELM regimes, are implemented, this deuterium control will facilitate control of the total plasma density. As described in section 9.2.1.2, achieving this control is critical for the development of low-collisionality operating regimes in NSTX-U.

9.2.2.5.1: Realtime Density Measurements

NSTX-U has two options for realtime density measurements. The first is a single chord FIR interferometer channel provided by UC-Davis collaborators as a new implementation of the FIReTIP diagnostic [64]. This chord is presently envisioned to be oriented toroidally, passing near the magnetic axis. Note that a conceptual design for density control using this diagnostic has already been developed and published [65]. If this diagnostic should not be available, the backup plan will be to use a realtime implementation of the Thomson scattering diagnostic (MPTS [66]). This has the advantage of better resolution of the full profile, especially at small major radius where the plasma resides during startup. However, the time resolution of the MPTS system (16.7 ms with two lasers, and 11.1 ms with a third laser upgrade) is significantly less than that of the FIReTIP system, which has sub-millisecond time resolution. Note that, as discussed in sections 9.2.2.1.1, realtime MPTS would accrue other benefits to PCS and NSTX operations in general, for instance, improved assessment of the pressure peaking factor and outer-gap if used as a constraint in rtEFIT. See chapter 10 for additional information on these diagnostics.

9.2.2.5.2: Conventional Gas Injectors

With regard to fueling actuators, initial operations in NSTX-U will use fueling from dedicated injectors on the low- and high-field sides of the machine. The low-field injectors are traditional piezo-electric injectors, and are generally used for the pre-fill and early ramp-up phase. They have characteristic opening/shut-off times of 5 ms. However, these injectors suffer from the well-known short-comings of low fueling efficiency due to the opacity of the SOL to injected neutrals, and loading of in-vessel surfaces with hydrogenic fuel.

H-mode access is generally provided by injection of gas from the high-field side [67], via a long tube running under the graphite tiles to the inboard midplane; the characteristics shut-off times of these valves are 10s of ms. Compared to the implementation in NSTX, this fueling line will be 2 times larger in diameter in NSTX-U. Furthermore, NSTX-U will not only have injectors at the

midplane and CS top (the "shoulder injector"), but also a high-field side injector half-way between the midplane and top. These changes will facilitate density control by allowing these tubes to pump out more quickly during the discharge.

Finally, two other "conventional" gas injection systems will be used on NSTX-U. A divertor gas injection system will be available, composed of two piezoelectric valves in the lower and in the upper divertor with orifices located in bull-nose tiles at the CHI gap. This system is primarily designed for radiative divertor studies, but could also be used for fueling studies. A massive gas injection (MGI) system for disruption mitigation studies will also be implemented. See section 2.2.3.3 for more information on this system.

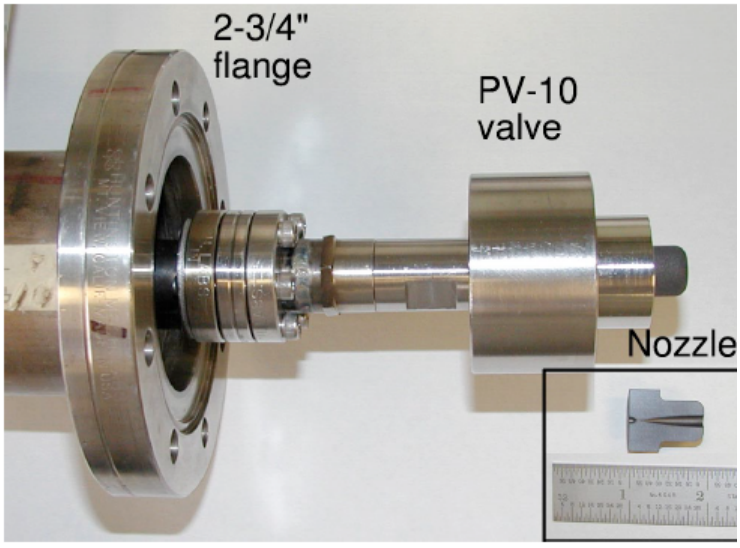

Fig. 9.16: Photograph of the SGI nozzle. The stainless steel parts are covered in a CFC shroud.

9.2.2.5.3: Supersonic Gas Injectors

The long time response of the high-field side fueling system and the low fueling efficiency of the low-field side injectors motivate the inclusion of advanced fueling systems in NSTX-U. In particular, it is desirable to minimize the amount of gas that enters the torus but does not fuel the main plasma. To this end, a supersonic gas injector (SGI) has been developed for fueling and diagnostic applications on NSTX and NSTX-U [68]. It is comprised of a graphite converging-diverging Laval nozzle and a commercial piezoelectric gas valve mounted on a movable probe on low field side midplane port. The SGI flow rate is up to 4 x 10^{21} particles/s, comparable to conventional NSTX gas injectors. The nozzle operates in a pulsed regime at room temperature with a reservoir gas pressure up to 0.33 MPa. The deuterium jet Mach number of about 4, and the divergence half-angle of 5^{o} - 25^{o}, have been measured in laboratory experiments simulating NSTX environment. Fueling efficiencies in the range 0.1 - 0.3 has been obtained from the plasma electron inventory analysis, compared to values of 0.02-0.1 using conventional injectors. This system will be integrated with the NSTX-U plasma control system, allowing it to be used for feedback applications

It is planned to develop routine use of SGI, in support of plasma operations on NSTX-U. In initial years, H-mode fueling scenarios with SGI fueling will be developed. A primary benefit of the SGI is a precise control of injected gas inventory. The SGI will support H-mode density limit

and pedestal studies, as well as perturbative transport experiments. In later years, it is planned to integrate the SGI in a feedback-control loop for active density control with PCS.

If, in the latter years of the research program, it appears that greater flexibility in fueling would be beneficial, the use of a cryogenic SGI (also known as a molecular beam/cluster injector) will be considered. Fueling efficiencies in the range of 30-60% have been observed with this technology on HL-2A [69]. Recent fueling experiments in LTX [70] indicate that cryogenic SGI can maintain high fueling efficiency even when placed far from the last closed magnetic surface; conventional SGI systems must have the nozzle near the plasma to maintain high efficiency. The increased gap between the nozzle and the plasma may prove advantageous as the total input power and pulse durations are increased. The need for such injectors, and any plans for implementation, will be assessed in conjunction with researchers from LTX, where such systems have already been developed.

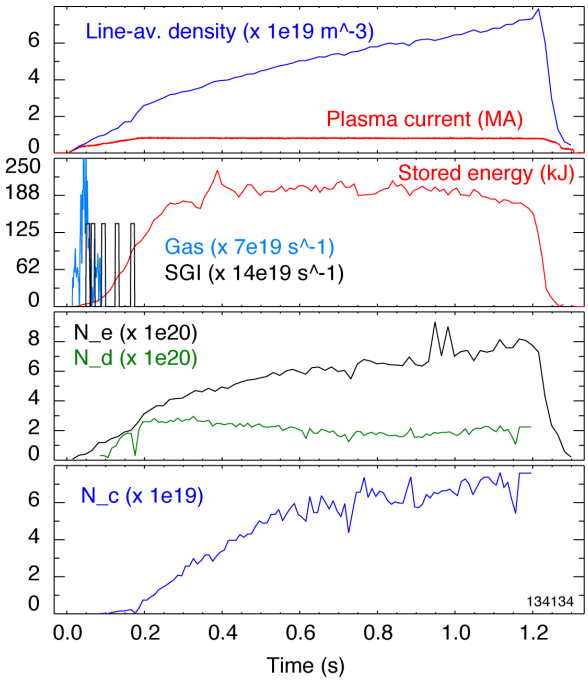

Fig.9.17: Example of deuterium inventory control using SGI and lithium pumping in a high-performance NSTX discharge. Shown from top to bottom are the line average density and the plasma current, the stored energy and gas fueling, the electron and deuteron inventories, and the carbon inventory.

9.2.2.5.4: Pumping Schemes

For deuterium pumping, NSTX-U will initially rely on lithium coatings. Note that as shown in Fig. 9.17, the combinations of actuators (low-field side fueling from the super-sonic gas injector, lithium pumping) available in the early phase of NSTX-U operation has already proven capable of producing a controlled deuterium inventory; it is the impurity accumulation that contributes to the rising electron inventory. Similar results have also been attained using traditional gas injection only. The cryo-pump will be installed between the 2nd and third years of operations, and is projected to provide sufficient deuterium pumping to meet the scenario development needs of NSTX-U. As described in Section 9.2.1.2 and the Boundary Physics chapter, various lithium coating systems and ELM pacing technologies will be used to control the impurity content in these scenarios.

9.2.2.5.5: Deuterium Inventory Control Plans

Density control experiments before the cryo-pump is installed will concentrate on the early phase of the discharge, using a PID-type controller to regulate the density. SGI will be used as the feedback actuator, and attempts will be made to develop reliable H-mode scenarios with minimal or no high-field side fueling. It is anticipated that this will facilitate improved early discharge reliability and the avoidance of early mode locking as in Fig. 9.5. This control development will be started as soon as either of the realtime density measurements are available, which may be as early as the first year in the case of the interferometer measurement.

Later experiments will use the cryo-pump to regulate the deuterium inventory. These experiments will first place the outer strikepoint in the vicinity of the cryo-pump entrance, and use the fueling feedback to control the density; both L-mode and H-mode density control will be assessed. Later experiments may, if necessary, incorporate the outer strike-point position in the density control loop, allowing the degree of pumping to be actively controlled. If successful, these combined fueling and pumping control schemes will be incorporated into the 100% non-inductive and high-current partial inductive scenarios described in section 9.2.1.

9.2.2.5.6: Research Plans by Year

The timeline for these efforts is as follows.

Year proceeding operations (2014):

- Implement PCS control of SGI.

Year 1 of operations (2015):

- Establish H-mode schemes with SGI and minimal high field side fueling.

Year 2 of operations (2016):

- Begin density feedback control development with realtime density measurements provided by interferometry (if available).

Years 3-4 of operations (2017-2018):

- Examine molecular cluster injector for advanced fueling applications.
- If interferometry is not available, then begin density feedback studies using realtime MPTS.
- Optimize combinations of cryo-pump and feedback controlled fueling to produce controlled density throughout the discharge.

9.2.3 Thrust 3: Disruption Avoidance By Emergency Stop Development

The three other thrusts in this chapter, and the research in the solenoid-free start-up group (Chapter 8), address key questions regarding plasma sustainment. However, the discharge is only complete when the stored energy and plasma current have been returned to zero. Developing the means to reliably compete this task is the subject of this section. This research program is divided into two complementary topics: detection of the need to terminate the discharge, and the actual rampdown sequencing.

This research complements the disruption avoidance techniques being developed in the MS TSG (Chapter 2), which aim to:

- develop MHD control techniques to avoid the need to terminate the discharge before the programmed rampdown, and
- develop the physics understanding of disruption mitigation techniques such as massive gas injection (MGI), and provide that technology as a potential actuator for disruption mitigation in NSTX-U if that is desired.

9.2.3.1 Realtime Determination of Need for Discharge Termination

The first step in this research sequence is to develop the necessary control system capability to determine when a discharge needs to be ramped down. Some of the necessary triggering events come from direct plasma diagnostic indicators of imminent disruption, while others are related to observation of infrastructure signals. These will be described in the following two sub-sections.

9.2.3.1.1: Engineering Indicators

In the first two years of the research program, NSTX PCS development will include the capability to automatically ramp-down the discharge based on certain non-disruptive indicators, in the hope of preventing the plasma from ever entering a disruptive state. The implementation of these indicators will include the following:

- The discharge will be ramped down before the solenoid coil reaches its current or force limit, based on extrapolation of the current waveform using the present loop voltage.
- The discharge will be ramped down if any coil systems are approaching their heating limit.

- The discharge will be ramped down if the value of χ^2 from rtEFIT is too high for a significant duration, indicating that the equilibrium reconstructions from which the shape control is derived are cannot be trusted.
- The physics operator will be able to initiate a rampdown with a single PCS waveform.

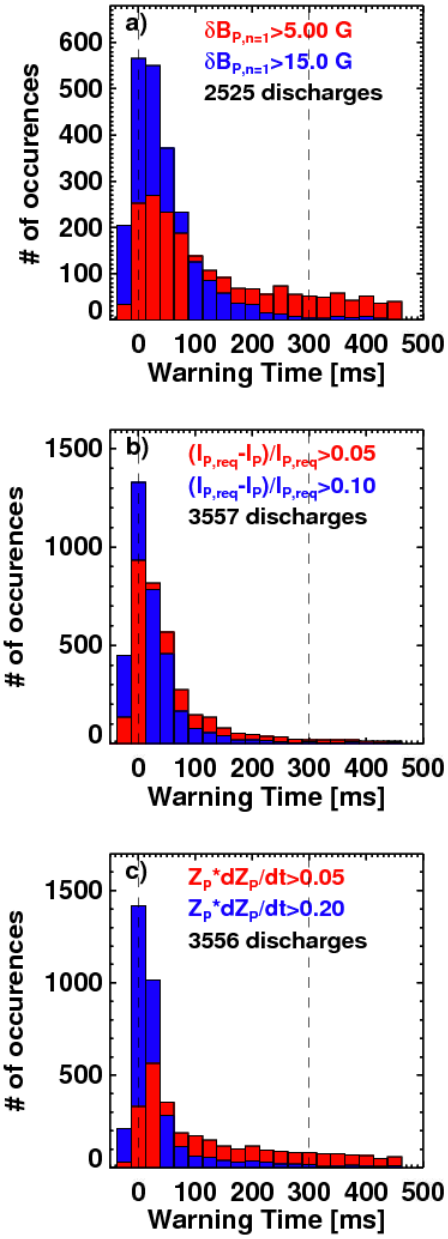

Fig 9.18: Histograms of warning times provided by threshold tests on a) the n=1 B_P amplitude, b) the plasma current deviation, and c) a measure of the vertical motion of the plasma column.

9.2.3.1.2: Data-Based Disruption Indicators

In the first two years of the research phase, ASC researchers and the MS stability group will also begin the implementation of realtime disruption detection algorithm. The initial realtime implementation will utilize the three signals in Fig. 9.18: the n=1 RWM amplitude, the plasma current deviation, and a vertical motion indicator. These diagnostics have the advantage of being already implemented in PCS, so that their output can be used for this disruption purpose immediately. The output of this disruption detector will likely be used to trigger a "fast-rampdown" of the plasma current and stored energy. Note that the data mentioned in this section are described in more detail in Ref. [71].

Fig. 9.18 shows histograms of the time between when one of these signals crosses a given threshold value and when the current quench occurs; this time is called the "warning time". Considering the n=1 B_P sensors in frame a), it can be seen that setting a threshold of 5G results in an unacceptable fraction of false positives, defined as cases where the threshold is crossed more than 300 ms before the current quench occurs. On the other hand, a threshold of 15 G results in elimination of most false positives, albeit with a significant increase in the number of late warnings. Frame b) shows a similar plot, where the quantity under consideration $\left(I_{P,req} - I_P\right)/I_{P,req}$ captures the extent to which the plasma current is less than the request; there is often a 10-30% loss

of plasma current in the phase preceding a disruption, which can be used for disruption detection. In this case, it is clear that a plasma current loss of more than 10% of the request is a good predictor of disruption. Finally frame c) shows disruption detection based on the quantity $Z_P \cdot dZ_P/dt$. This quantity has the benefit of being large when the plasma is above the midplane and moving upward rapidly, or below the midplane and moving downward rapidly. A threshold of 0.05 m^2/s results in detection with a large fraction of false positives, while increasing the threshold to 0.2 results in a reasonable disruption detector.

While the previously mentioned tests can provide a solid basis for disruption detection early in the research program, it will likely be necessary to add additional tests if the goal is to detect all disruptions with a minimal number of false positives. To this end, additional diagnostic indicators have been examined, to determine what signals should be brought in to the system in realtime.

Examples of three additional indicators are shown in Fig. 9.19, Frame a) shows an example where the ratio of measured to modeled neutron emission is used as an indicator, based on the observation that there are often large fast-particle losses due to MHD modes [72] in the phase proceeding a disruption. The neutron emission is predicted using a simple slowing down models, using n_e, T_e, and Z_{eff} measurements as input. This figure shows that the having the neutron emission drop beneath 50% of the model prediction is a good indicator of imminent disruptions. Fig. 9.19b) shows that having the core rotation drop beneath ~3.5 kHz is a good indicator of disruption; both RWMs or n=1 core/kink modes that lock to the wall contribute to these statistics. Finally, disruptions are often preceded by a rapid reduction of particle confinement, manifest as a drop in the line density. Fig. 9.19c) shows that dn_e/dt beneath $\sim -3\times10^{14}$ $1/cm^2s$ is a good indicator of imminent disruptions. These diagnostics required to implement these tests in realtime (realtime rotation, realtime Thomson scattering), are not presently available at NSTX. However, a realtime rotation diagnostic is likely to be available from the 2nd year of the research program, and a realtime Thomson scattering diagnostic may also be implemented in later years.

In order to use these many disruption indicators, it will be necessary to combine the information from the various tests. This has often been done via a neural networks (see Ref. [73] and references therein). However, NSTX researchers have explored an alternative scheme [71]. In this scheme, a series of ~15 threshold tests as defined above are evaluated at each time-slice. For each of the ~15 tests, various "point" totals are assigned to various threshold values. For instance, 1 point might be assigned for the B_P n=1 signal exceeding 5 G, 2 points for it exceeding 10 G, and 3 points for exceeding 15 G; similar assignments of point values to various thresholds have been made for all the tests. At each time step, all of the threshold tests are evaluated and the points from all tests are summed to make the aggregate point total. When this aggregate point total exceeds a given value, a disruption warning is declared.

An example distribution of warning times from these compound detection algorithms is given in Fig. 9.20, for an aggregate point total of 9 required for disruption. With this formulation, ~2.5% of disruptions have the warning declared "late", defined here as after the time 10 ms before the current quench. Approximately 3.4% of disruptions have "false positives", where the warning is more than 300 ms before the current quench. The remainder of disruptions (94%), have the disruption warning declared within 10 ms of the current quench, but not more than 300 ms before.

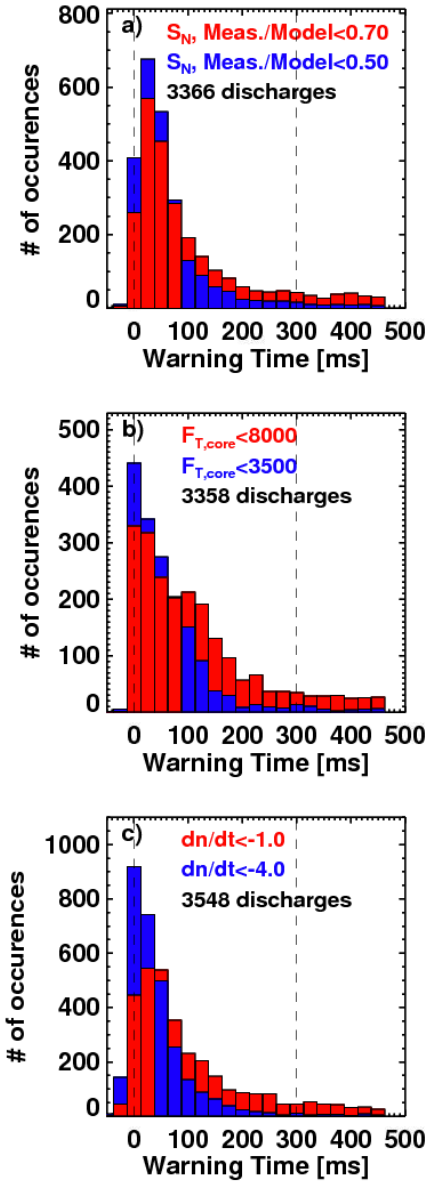

Fig. 9.19: Disruption warning time histograms, using as diagnostic indicators a) the ratio of measured to modeled neutron rate, b) the core rotation frequency, and c) the time derivative of the line-density.

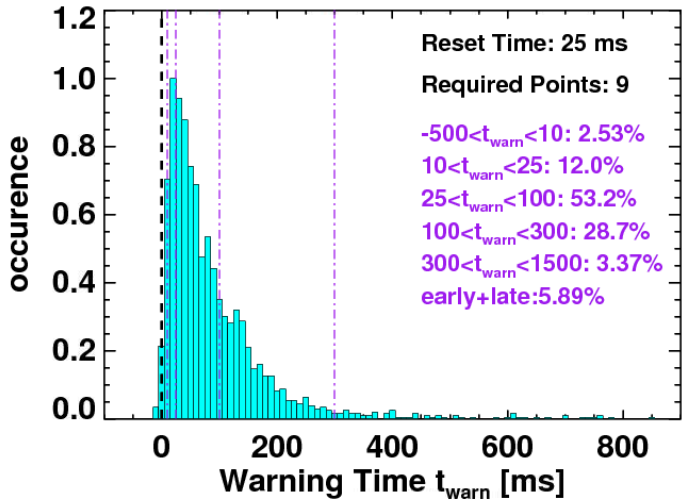

Fig 9.20: Histogram of disruption warning times using the compound disruption warning algorithm.

It is interesting to consider the sources of those false positives and missed warnings. A large fraction of the false positives are due to rotating MHD mode that slow the plasma rotation, and sometimes even lock to the wall. These are generally disruptive events, with alarms being generated due to the slowed rotation and large mode amplitudes, but the plasma does on rare occasion survive, reheat, and continue on with the discharge. The missed-warnings are dominated by rapidly growing ideal and resistive wall modes. Hence, improved control and early detection of these modes will be critical for avoiding unmitigated disruption

Future research will further establish which of the diagnostics beyond those in Fig. 9.18 & 9.19 are most important for improving the detection fidelity. These will then be translated into requirements for additional realtime diagnostics to be implemented in the later phase of the research period. These new diagnostics will be incorporated into a disruption detection algorithm, either similar to that described here, or new algorithms determined through further research.

9.2.3.1.3: Physics-Based Disruption Indicators

The methods above utilize a rather simple interpretation of the in-vessel RWM sensors for mode detection: a simple Fourier analysis is utilized to determine the n=1 distortion amplitude and phase, and a series of threshold on the distortion amplitude is defined. While this procedure generally works well, it does result in some fraction of missed disruptions. Fortuitously, as described in section 2.2.1.3, research in the macro-stability group has resulted in a state-space RWM controller [74], which can be used for disruption detection applications in addition to the feedback control role (described in more detail in section 2.2.3.1.3).

The state space controller uses a physics model for the resistive wall mode eigenfunction and plasma response, as well as a model for the 3-dimensional conducting structures in NSTX. The controller is being expanded for NSTX-U to allow independent control of the midplane RWM coil set, as well as multiple RWM eigenfunctions. The real-time computation of a model for the expected field measured by the RWM sensors (the "observer") allows the controller to determine when the differences between the modeled and measured signals are sufficiently large that feedback is no longer likely to stabilize the modes. When this occurs, a "Loss of Control" alarm will be declared, resulting in the appropriate rapid shut-down or MGI mitigation.

Similarly, the description in 9.2.3.1.2 relies on detection of plasma motion for assessing vertical stability. However, more first-principle measures of loss of vertical control will be assessed, based on the calculations described in section 9.2.2.2.2. For instance, realtime calculations of the field index will be assessed as an indicator of approaching the limits of vertical control. More sophisticated realtime evaluations of the growth rate will also be examined, for instance, with a c-language implementation of the Gspert code or relay feedback measurements. These measures will be used to determine when the limits of vertical control have been approached, and shut-down of the plasma is required.

9.2.3.2: Soft- and Hard-Stop Sequence Development

Once it is determined that the plasma discharge must be terminated, a complicated sequence of events, using multiple actuators, must be initiated. Clearly, the plasma current must be ramped down. Additionally, the heating power should be reduced sufficiently fast to reduce the plasma

energy content, but not so fast as to trigger rapid back-transitions and disruptions. The plasma shaping should be reduced, in order to prevent vertical instabilities if the internal inductance rises. It may be desirable to increase the gas fueling as well.

To begin this development, a PCS algorithm containing the rampdown initiating capabilities of 9.2.3.1 will be implemented. It appears that the tests in 9.2.3.1.1 will be used to trigger a transition to a "slow rampdown" sequence, while the disruption tests in 9.2.3.1.2 will trigger a transition to a "fast rampdown" sequence. The tests in section 9.2.3.1.3 may trigger either of these sequences. The software for developing these alarms will likely be based on the "alarm" category presently in use at DIII-D, but with modifications to increase its generality. This new alarm category will do the evaluations noted above, and at the appropriate time, issues "phase sequence changes" to the PCS code controlling the various relevant actuators (beams, PF coils, OH coil, etc.) This in turn will initiate the appropriate sequence of actions for each of these actuators.

In the first years of NSTX-U research, the basic parameters of the two rampdown sequences will be established. For the slow-rampdown sequence, which presumes that the health of the plasma is good at the start of the rampdown, a stored energy rampdown and de-shaping step will likely start the rampdown sequence. This will be followed by a reduction of the plasma current. Of course, the detection of a disruption during this phase can lead to a transition to the fast rampdown sequence.

In the fast rampdown sequence, the plasma health has already degraded to the point where a disruption is considered imminent. The timing intricacies of the "slow rampdown" sequence will likely be avoided, with deshaping and energy and current rampdowns beginning immediately. Efforts during the first years will demonstrate under what circumstances this method works. For instance, experiments will indicate circumstances when the fast rampdown sequence will bring the current down smoothly, compared to cases where the initiation of the rampdown accelerates the disruption. Those latter cases will eventually become a third branch in the rampdown scheme, trigger a mitigation method such as massive gas injection (MGI).

There is an effort in the MS group to develop massive gas injection for rapid discharge shutdown; this research program is described in thrust MS-3. As that system matures, it will be brought into this shutdown scheme as an additional branch, where MGI can be triggered based on information from the disruption detection algorithms. Note that triggering MGI while the neutral beams are injecting will not be allowed, as the increased neutral pressure can result in enhanced beam reionization in the drift duct and localized damage to the duct or vessel. With the PCS, the beams will be turned off before the MGI is triggered, preventing this potential problem.

This would allow closed-loop MGI testing, and possibly even inclusion of MGI as a routine on-line system if that is found to be desirable.

9.2.3.3: Research Plans By Year

The time-scale for these automated ramp-down experiments under the baseline budget scenario is presented in the following list. Under incremental funding, this research plan could be significantly accelerated by the additional run-time and improved realtime diagnostics (real-time MPTS earlier, real-time rotating MHD signals, realtime bolometry).

Year 1 of operations (2015):

- Implement the formulation for declaring "alarms" in PCS. These alarms will be useful for soft-stop automations, as well as general event handling in PCS.
- Implement simple algorithms to detect the need for discharge shut-down.

Year 2 of operations (2016):

- Begin development of slow- and fast- rampdown sequence

Year 3-4 of operations (2017-2018):

- Improve disruption detection schemes, including additional realtime diagnostics.
- Complete development of ramp-down sequences, and assess circumstances when these rampdown methods are insufficiently fast to interdict the disruption.
- Use the disruption detection algorithm to trigger MGI.
- Assess and implement realtime measures of vertical stability.

9.2.4 Thrust 4: Exploration of Scenario Physics of Next Step STs

Thrusts 1 through 3 described above are designed around the extensive capabilities of the NSTX-Upgrade facility. For instance, Thrust #1 attempts to optimize scenarios in NSTX-U, Thrust #2 develops control strategies with the NSTX-U actuators, and Thrust #3 develops strategies for ramping down or otherwise terminating NSTX-U discharges. However, there will be scenario research for next-step STs that is not captured in these thrusts, for instance, research exploring the basic physics leading to advanced scenarios. These research elements are captured in this fourth research thrust.

9.2.4.1: Optimal Profiles for High-β_N Steady State

9.2.4.1.1: Research Description

As described in the introduction to Section 9.2.2.3, there may be conflicting demands in determining the optimal current and rotation profiles. For instance, elevating q_{min} may be good for core stability, but deleterious for confinement. Increasing the rotation is generally beneficial,

but the optimal details of the profile shape, including the effects on tearing modes, RWMs, and micro-turbulence, remains a question for research. Both q-shear and rotation at the edge may impact the pedestal parameters. Focused experiments in the BP, MS and T&T TSGs will address each of these issues in detail, though often in lower-performance scenarios designed to improve diagnostic access or ease modeling. However, it remains a task for the ASC TSG to integrate these results.

Experiments in the later phase of the research period will address this question of optimal profiles, building on results from the first years in the following sense. The focused physics experiments in the other TSGs will give clear indication of the optimal profiles for any single goal, for instance, transport reduction or core n=1 mode stability. The control development described in Section 9.2.3.2 will additionally provide a first look at some of the underlying physics. For instance, the q_{min} control experiments will provide first data on how confinement and stability varies with q_{min}, while the rotation control experiments will provide data on how rotation impacts those two quantities.

Previously developed high-performance scenarios, likely with near-100% non-inductive current drive and strong boundary shaping, will be used for dedicated experiments. Controlled scans of the core or edge rotation with approximately fixed safety factor, and core and edge safety factor with approximately fixed rotation, will be conducted, at various values of β_N. It is likely that the non-inductive fraction or even the current level will vary in these cases, which is an acceptable compromise given realistic actuator constraints. The turbulence characteristics, global confinement, and global stability will be documented, the latter potentially via resonant field amplification (RFA) measurements [74,75] The outcome will be an improved experimental understanding of what profiles lead to simultaneously high-confinement and high β-limits. These experiments will also provide an excellent set of benchmarking discharges for the integrated modeling described in section 9.2.4.3.

This chapter is largely written in the context of standard H-mode scenarios, which provided the basis for nearly all NSTX experimental operations and the modeling described previously in this chapter. However, there may be other beneficial regimes of operation, as partially described in the boundary physics chapter, section 4.2.2. These include I-mode [76,77], regimes with internal transport barriers [78,79], and the "Enhanced Pedestal H-mode" (EPH) [80]. The last of these (EPH) is likely the most attractive for future ST development, as, in contrast to the first two, it tends to reduce the pressure peaking factor. If it appears practical, these regimes will be examined from the standpoint of developing integrated long-pulse scenarios.

9.2.4.1.2: Research Plans by Year

The research program in the area of profile optimization will have dedicated experiments weighted towards the later years, and be executed in conjunction with the T&T, BP, and MS topical science groups.

Years 1 and 2 of operations (2015-2016):

- Examine data collected from the q_{min} control experiments (at fixed I_P) to understand the confinement dependencies on q_{min}.

Years 3-4 of operations (2017-2018):

- Augment data from previous scans to complete scans of rotation, q_{min}, and q_{95}. Use data to determine optimal safety factor for next-step STs.
- Exploit research on alternative pedestal scenarios (EPH, I-mode) to develop scenarios if that research appears creditable.

9.2.4.2: Range of Validity for Classical Neutral Beam Current Drive Calculations

9.2.4.2.1: Research Description

Many of the calculations discussed above rely on the assumption that the fast ion slowing down, radial transport, and net current are determined by (neo)classical processes. However, this assumption is not always valid in the experiment. For instance, chirping TAEs and fishbone modes are known to provide anomalous transport or slowing down of the fast ions [81], and can modify the current profile [10]. Understanding the regimes in which deviations from classical behavior are observed, and the magnitude of those deviations, are critical for projecting equilibrium scenarios for ST FNSF devices.

Research in the first few years of NSTX-U operations will, in conjunction with the Energetic Particle physics research group, attempt to understand the circumstances where beam current drive is anomalous. To begin with, beam blip experiments with the new and old sources will be conducted to better understand the confinement and prompt loss of the injected fast ions, following the methodologies in Refs. [72,82]. Following this, scans of the relevant parameters (plasma density, beam voltage and tangency radius) will be conducted under the relevant high-performance H-mode discharge conditions; these scans may be accomplished as part of the q_{min} control validation experiments described in section 9.2.2.4.1, in which case they would be augmented with additional required data. The neutral beam current drive and fast ion distribution will be inferred by comparing TRANSP simulations to reconstructions of the current profile,

neutron emissions rates, FIDA signals, and fusion product rates. Any anomalies in the fast ion physics will be correlated with the plasma parameters and observed MHD activity.

Following this phase of physics study, experiments will attempt to exploit any observed non-classical behavior for improved scenarios. An example of such scenario improvement is shown in the right-hand column of Figure 9.3, where the confinement and density dependence of the non-inductive current drive sources are shown for an I_P=1.0 MA, B_T=1.0T, P_{inj}=12.6 MW with a spatially uniform anomalous fast ion diffusivity D_{FI} of 1 m^2/s. This value is roughly consistent with the largest values inferred during MHD quiescent phases in NSTX high-performance discharges [10]. This column of figures should be compared to the left column of the figure, previously discussed in the context of Section 9.2.1.1, which has no imposed fast ion diffusivity.

As might be expected, the fast ion diffusion has essentially no effect on the bootstrap current level in Fig. 9.2e). However, the central beam current drive at low density, on the left of frame f), is reduced when the fast ion diffusivity is imposed. This causes the confinement required for full non-inductive current drive in Fig. 9.2g) to increase at low density, to make up for the lost current drive. Alternatively, at lower density, the non-inductive current level for $H_{98(y,2)}$=1 will be reduced due to the loss of beam current drive.

Countering this negative result, however, is the observation in Fig. 9.2h) that q_{min} is maintained above unity over the entire range of density and confinement. This implies that the low-density limit apparently imposed in Fig 9.2d) by the onset of core n=1 MHD as q_{min} approaches 1 is eliminated in this case. Additionally, Ref [19] shows that the total pressure peaking is reduced in this case with imposed fast ion diffusivity. This has the result of improving the global stability limits, and DCON calculations indicate that, with an ideally conducting wall at the location of the NSTX passive plates, all idea n=1 modes are stable. Hence, at the expense of a reduction in current drive efficiency, a fast ion diffusivity of $1m^2/s$ results in a significant expansion of the stable operating space.

These trends are further emphasized in Fig. 9.21, where parameters of B_T=1.0 T, I_P=1.0 MA, P_{inj}=12.6 MW, f_{GW}=0.7 scenarios are shown as a function of applied fast ion diffusivity; these parameters are those near the center of the space illustrated in Fig. 9.2. As noted above, values of to ~1 m^2/s are consistent with the values inferred from MHD quiescent phases in NSTX while D_{FI}=~4 m^2/s is roughly consistent [19] with that observed in a single discharge with a string of rapid TAE avalanches [10]. It is clear from frame a) that increasing D_{FI} from 0 to 1 m^2/s reduces the central NBCD by almost a factor of 2, and that the increase to D_{fi}=4 m^2/s reduces it by half again. Fig 9.21b) shows the rapid drop in total pressure peaking with non-zero D_{FI}, an effect that tends to taper off above D_{FI}~3 m^2/s. The minimum safety factor also has the largest variation for smaller values of D_{fi}, varying from 1.25 all the way to 2 of the range of D_{FI} shown. The non-

inductive current fraction drops from 91% to 65%. Note that this strong sensitivity of the equilibrium parameters to small values of D_{FI} provides a sensitive test of the fast-ion behavior.

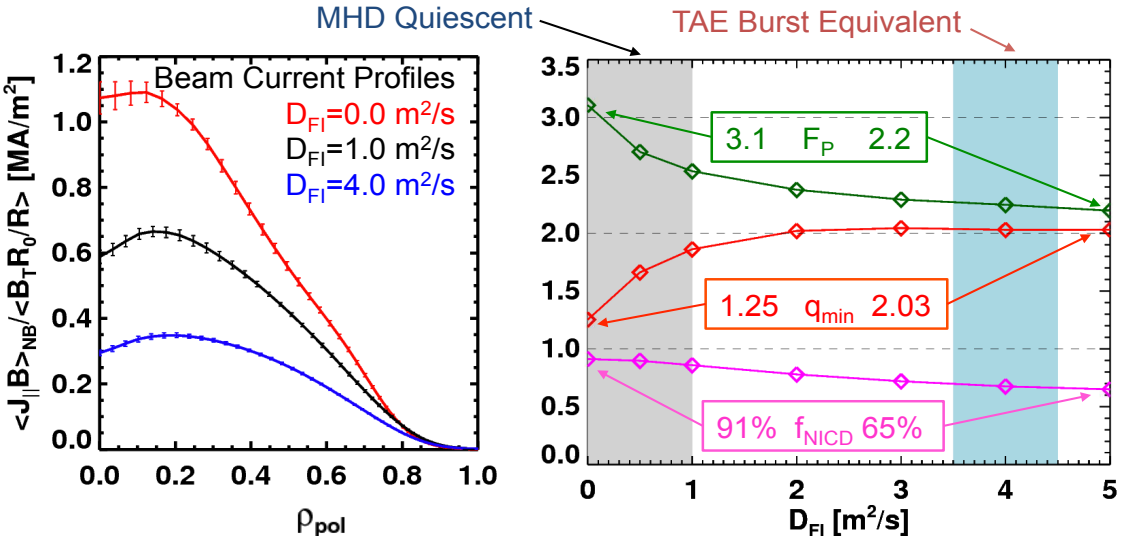

Fig. 9.21: Effect of $D_{FI}\neq 0$ on the NBCD profile (left), and on the pressure peaking (F_P), minimum safety factor, and non-inductive current fraction (right).

Regimes where Alfvénic activity was used to elevate q_{min} have been observed in DIII-D [83,84]. If similar physics can be used for control in NSTX-U, it may allow regimes with both lower density, and higher central heating power. Experiments in the final years will attempt to exploit this physics, in order to expand the high-performance operating space of NSTX-U.

9.2.4.2.2: Research Plans by Year

The research plan in this area, to be conducted in conjunction with the energetic particles research group, is as follows.

Year 1 of operations (2015):

- Make measurements of beam prompt loss and slowing down, for comparisons to TRANSP/NUBEAM calculations, over a range of beam and plasma parameters.
- Make first assessments of non-classical behavior using the q_{min} control experimental data.

Year 2 of operations (2016):

- Continue assessments of non-classical NBCD behavior, over a wide range of parameters.
- Begin comparisons of NSTX-U data to models of fast ion diffusion

Year 3-4 of operations (2017-2018):

- Continue comparisons of NSTX-U fast-ion data to models of fast ion diffusion.

- Develop, if appropriate, discharge scenarios that exploit anomalous fast ion diffusion in order to expand the high-performance operating space of NSTX-U.

9.2.4.3: Exploration and Validation of Integrated Models for FNSF and other Next-Step STs

The current drive simulations presented above are all based on calculations imposing the thermal profiles: the profile shapes are taken from experiment, and then scaled so that desired values of f_{GW} and H_{98} or H_{ST} are achieved. While this approach is useful for scenario development in NSTX & NSTX-U, where reasonable assumptions about the profile shapes and confinement levels can be made based on well documented discharges, it has insufficient predictive power for projecting scenarios for next-step STs. Rather, those projections ultimately require that the profiles of rotation, temperature, and current be modeled simultaneously, with realistic source and transport models.

Joint research between the BP, T&T, SFSU and ASC TSGs towards this end will proceed along converging paths in the proposed research program.

- The Boundary Physics group will work to develop an improved predictive understanding for the pedestal height and width. This will involve both empirical understanding of the pedestal scaling with engineering parameters (I_P, B_T, P_{inj},…), and first-principle model development and validation. This research is described in section 4.2.1.2.

- The Transport and Turbulence group will work to develop an improved predictive understanding of the core momentum and energy transport. This is an extremely complex research task, and involves the following elements. The 0D confinement trends with field current, and power, or alternatively q and υ^* will be examined in the first 2 years of NSTX-U operations; these will enable 0D projections to next-step STs with improved confidence. Next, reduced models such as TGLF will be tested against both non-linear transport simulations for NSTX-U and actual NSTX-U data; both the thermal, particle and momentum transport will be addressed, and the modified retuned if necessary. Simultaneously, electron thermal transport driven by *AE modes will be simulated, and semi-empirical models for the electron thermal transport will be developed, tested, and, if successful, incorporated into integrated predictions. This research is described in Chapter 3.

- As described in this chapter, the ASC research group, in close collaboration with energetic particle researchers, will validate the current drive predictions from codes such

as NUBEAM, and determine regimes where the (neo)classical models of fast ion current drive, slowing down, and radial transport are valid.

- Additionally, researchers will work to further refine the free-boundary equilibrium model in TRANSP. This model has already been used successfully in developing the large database of NSTX-U equilibria [19]. New capabilities include the coupling of the plasma current and PF coils to the resistive, assumed-axisymmetric, vacuum chamber, and control of the plasma boundary and current through voltage control of the PF & OH coils, using simplified power supply models. These capabilities will be especially critical when simulating the ramp-up and ramp-down of the current, a phase with large vacuum vessel currents and rapid shape variations.

Testing of these models will be an interactive process throughout the full 5-year research program. However, the focus on integrated testing of these models on the highest performance discharge scenarios will increase in the later years of the research campaign. For instance, if the core transport models cannot provide sufficient profile prediction, integrated pedestal and current drive calculations can be attempted, with prescribed core profiles. Alternatively, core transport models can be integrated with current drive calculations, using a prescribed pedestal structure. This research is facilitated by the improved multi-region capability in the PT-SOLVER upgrade to PTRANSP. In this way, progress towards integrated scenarios can be achieved even if one research area is not yet mature.

The modeling described in the previous paragraph will proceed in two steps. First, these integrated simulations will be applied to high-performance NSTX-U (and potentially MAST-Upgrade) scenarios, in order to validate the predictions. The targets for simulation will likely come from the most attractive 100% non-inductive scenarios described in section 4.2.1.1, and from the q- and rotation scans described in section 9.2.4.1. It is envisioned that some period of iteration between the integrated models and experiment will be required to improve agreement. This modeling will first focus on the steady, relaxed flat-top phase, and agreement between models and both 0D and 1D parameters will be examined. In parallel, the SFSU TSG, in collaboration with ASC, will be developing models for the plasma current ramp-up. As the two phases of the experimental discharges are brought together (see section 9.2.1.4), the modeling will also be combined.

Next, integrated simulations of next-step ST scenarios will be conducted. While the exact scenarios to be studied have not been identified, it is likely that they will be based on designs such as the PPPL pilot plant [5], PPPL FNSF [85], ORNL FNSF [2], or Culham CTF [4]. Key goals of these simulations will include determining the current drive requirements for achieving

non-inductive ramp-up and sustainment, predicting the pressure and rotation profiles for use in stability calculations, and assessing the fusion power and neutron wall loading for those devices.

9.3 Simulation Tools for Integrated Scenario Research and Control Development

Many codes are used for the development of advanced scenario plasmas and associated control systems. A summary of these codes is provided here:

9.3.1: TRANSP

The TRANSP code [86] is a critical tool for the understanding scenario physics in NSTX-U. It is described in detail in Section 3.4.1.4.

9.3.2: DCON

The DCON code provides rapid analysis of the low-n ideal stability of tokamak plasmas, and is useful for assessing the no-wall and with-wall stability limits. It is described in detail in Section 2.3.2.

9.3.3: TOKSYS

The TokSys is a modeling and simulation environment which allows closed loop simulation of the full Tokamak plasma and shape control system by connecting the plasma model to the Plasma Control System code through a simulation server (the “simserver”). While it is possible to connect different plasma models (e.g. the Corsica DIII-D model is connected to Toksys), TokSys contains its own finite element code to solve a non-rigid plasma response model based on the linearized Grad-Shafranov equation [50]. This model can be used for shape and position control development.

9.3.4: EFIT & LRDFIT:

EFIT [87] and LRDFIT [88] are codes used to construct experimental equilibria, constrained by experimental measurements of the external field and flux, measured pitch angles, and kinetic parameters. The implementation of EFIT for NSTX [89] is described in greater detail in Section 2.3.1.

9.3.5: NUBEAM

The NUBEAM [90] Monte-Carlo code is used to compute the neutral beam heating and current drive parameters for scenario development. It is generally used as a module within TRANSP, as described in Section 3.4.1.4.

9.3.6: Other Codes

Note that HHFW and EBW heating and current drive may become more important to advanced scenario research in the later years of the plan. These schemes have dedicated codes (TORIC, AORSA, GENRAY, CQL3D) that are described at the end of Chapter 7. Similarly, reduced transport models will be tested on high-performance discharges. The codes that manifest these models are discussed at the end of chapter 3.

9.4 Research Timeline

The projected research timeline under base funding is shown below. Under incremental funding, additional run-weeks and staff would allow the research program to be accelerated. Additionally, the more rapid transition to a high-Z first wall will provide more stringent tests of the scenario extrapolability to next-step ST devices.

There are a number of tasks summarized in by the phrase “Run Prep.” in this timeline. These include commissioning tasks done in tandem by the physics and engineering staffs, such as commissioning of the gas injection system, high-speed data links for the control system, and operations magnetic diagnostics, as well as upgrades to the plasma control system to support initial operations.

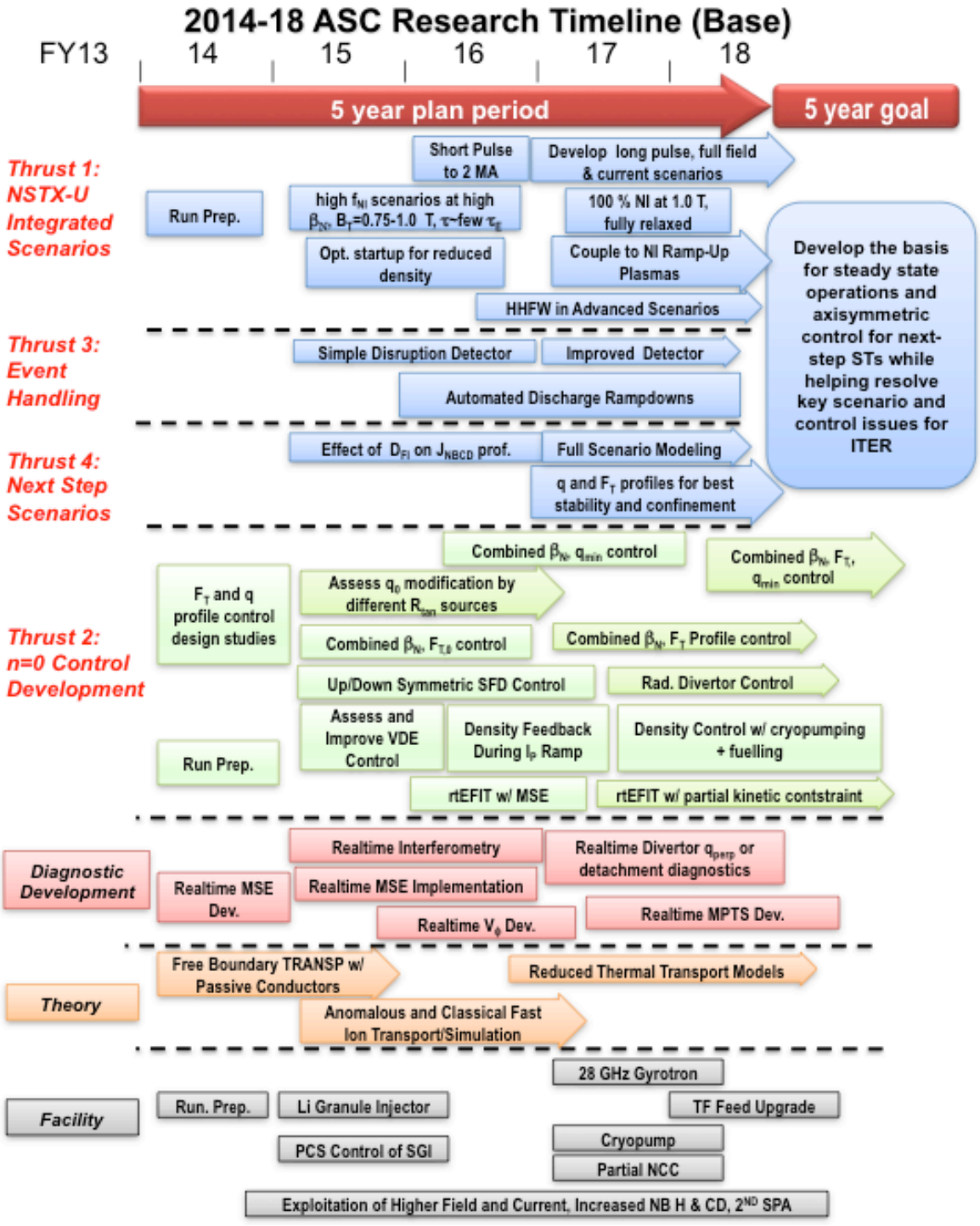
2014-18 ASC Research Timeline (Base)
FY13
14
15
16
17
18
5 year plan period
5 year goal
Thrust 1: NSTX-U Integrated Scenarios
Short Pulse to 2 MA
Develop long pulse, full field & current scenarios
Run Prep.
high f_{NI} scenarios at high β_N, B_T=0.75-1.0 T, τ~few τ_E
100 % NI at 1.0 T, fully relaxed
Opt. startup for reduced density
Couple to NI Ramp-Up Plasmas
HHFW in Advanced Scenarios
Develop the basis for steady state operations and axisymmetric control for next-step STs while helping resolve key scenario and control issues for ITER
Thrust 3: Event Handling
Simple Disruption Detector
Improved Detector
Automated Discharge Rampdowns
Thrust 4: Next Step Scenarios
Effect of D_{FI} on J_{NBCD} prof.
Full Scenario Modeling
q and F_T profiles for best stability and confinement
Thrust 2: n=0 Control Development
Combined β_N, q_{min} control
Combined β_N, $F_{T,}$ q_{min} control
F_T and q profile control design studies
Assess q_0 modification by different R_{sep} sources
Combined β_N, $F_{T,0}$ control
Combined β_N, F_T Profile control
Up/Down Symmetric SFD Control
Rad. Divertor Control
Assess and Improve VDE Control
Density Feedback During I_p Ramp
Density Control w/ cryopumping + fuelling
Run Prep.
rtEFIT w/ MSE
rtEFIT w/ partial kinetic contstraint
Diagnostic Development
Realtime Interferometry
Realtime Divertor q_{perp} or detachment diagnostics
Realtime MSE Dev.
Realtime MSE Implementation
Realtime V_ϕ Dev.
Realtime MPTS Dev.
Theory
Free Boundary TRANSP w/ Passive Conductors
Reduced Thermal Transport Models
Anomalous and Classical Fast Ion Transport/Simulation
Facility
28 GHz Gyrotron
Run. Prep.
Li Granule Injector
TF Feed Upgrade
PCS Control of SGI
Cryopump
Partial NCC
Exploitation of Higher Field and Current, Increased NB H & CD, 2ND SPA

References

[1] Y.-K. M. Peng, et al., Plasma Phys. Control. Fusion **47** (2005) B263.
[2] Y.-K. M. Peng, et al, Fusion Science and Technology **56** (2009) 957.
[3] R.D. Stambaugh, et al., *Candidates for a Fusion Nuclear Science Facility (FDF and ST-CTF),* Paper P2.110, 37th EPS Conference on Plasma Physics, Dublin, Ireland (2010), http://ocs.ciemat.es/EPS2010PAP/pdf/P2.110.pdf.
[4] G.M. Voss, et al., Fusion Eng. and Design **83** (2009) 1648.
[5] J.E. Menard, et al., Nuclear Fusion **51** (2011) 103014.
[6] F. Najmabadi & the ARIES team, Fusion Engineering and Design **65** (2003) 143.
[7] H.R. Wilson, et al., Nuclear Fusion **44** (2004) 917.
[8] S.P. Gerhardt, et al., Nuclear Fusion **51** (2011) 073031.
[9] J.E. Menard, et al., Phys. Rev. Lett **97** (2006) 095002.
[10] S.P. Gerhardt, et al., Nuclear Fusion **51** (2011) 033004.
[11] J.E. Menard, et al., Nuclear Fusion **52** (2012) 083015.
[12] D. Ryutov, Phys. Plasmas **14** (2007) 64502.
[13] D. Ryutov, et al., Phys. Plasmas **15** (2008) 092501.
[14] V.A. Soukhanovskii, et al., Nuclear Fusion **51** (2011) 012001.
[15] V.A. Soukhanovskii, et al, Phys. Plasmas **19** (2012) 082504.
[16] S.L. Allen, et al., *Results From Initial Snowflake Divertor Physics Studies on DIII-D*, IAEA FEC, San Diego, CA (2012).
[17] V.A. Soukhanovskii, et al., Phys. Plasmas **16** (2009) 022501.
[18] V.A. Soukhanovskii, et al., Nuclear Fusion **49** (2009) 095025.
[19] S. P. Gerhardt, et al., Nuclear Fusion **52** (2012) 083020.
[20] D.A. Gates, et al., Phys. Plasmas **13** (2006) 056122.
[21] D.A. Gates, et al., Nuclear Fusion **46** (2006) S22.
[22] S.M. Kaye, et al., Nuclear Fusion **46** (2006) 848.
[23] J.E. Menard, et al., Nuclear Fusion **45** (2005) 539.
[24] I.T. Chapman, et al., Nuclear Fusion **50** (2010) 052002
[25] I. T. Chapman, et al. Nuclear Fusion **51** (2011) 073040.
[26] J. Breslau, et al., Nuclear Fusion **51** (2011) 063027.
[27] S.P. Gerhardt, et al., Nuclear Fusion **53** (2013) 043020.
[28] J.E. Menard, et al. Nuclear Fusion **50** (2010) 045008.
[29] J.M. Canik, et al., Nuclear Fusion **50** (2010) 064016.
[30] S.P. Gerhardt, et al., Nuclear Fusion **50** (2010) 064015.
[31] J. Roth, et al., Journal of Nuclear Materials **122 & 123** (1984) 1447.
[32] See figure on page 8 of NSTX-U engineering calculation NSTXU-CALC-11-03-00, by K. Tresemer.

[33] J. Hosea, et al. Phys. Plasmas **15** (2008) 056104 (2008).
[34] D. Liu, et al., Plasma Phys. Control. Fusion **52** (2010) 025006.
[35] D. Gates, et al., Fusion Engineering and Design **81** (2006) 1911.
[36] D. Mastrovito, et al, Fusion Engineering and Design **85** (2010) 447.
[37] B.G. Penaflor, et al., *A structured architecture for advanced plasma control experiments*, Proc. 19th Symp. On Fusion Technology (Lisbon, Portugal) (16-20 September) p. 965 (1996).
[38] B.G. Penaflor, et al., Fusion Engineering and Design **71** (2004) 47.
[39] S.P. Gerhardt, et al., Fusion Sci. and Tech. **61** (2012) 11.
[40] J.R. Ferron, et al., Nuclear Fusion **38** (1998) 1055.
[41] D.A. Gates, et al., Nuclear Fusion **46** (2006) 17.
[42] E. Kolemen, et al., Nuclear Fusion **50** (2010) 105010.
[43] E. Kolemen, et al., Nuclear Fusion **51** (2011) 113024.
[44] S. A. Sabbagh, et al., Nuclear Fusion **46** (2006) 635.
[45] B. Wu et al., *Plasma vertical position control simulation of EAST Tokamak,* 31st EPS Conference on Plasma Phys. London, 28 June - 2 July 2004 ECA Vol.28G, P-5.131 (2004).
[46] E. Schuster, et al., Automatica **41** (2005) 1173.
[47] L. Scibile and B. Kouvaritakis, IEEE Transactions on Control Systems Technology **9** (2001) 148.
[48] S. Majhi, and D. P. Atherton. "Online tuning of controllers for an unstable FOPDT process." Control Theory and Applications, IEE Proceedings **147** (2000) 421.
[49] E. Kolemen et al., "*Vertical Stability of NSTX and NSTX-U*", 24th IAEA Fusion Energy Conference, October, 2012, # EX/P4-28.
[50] A. Welander et al., *Linear Plasma Response Model Based on the Solution to a Perturbed Grad-Shafranov Equation*, 52nd APS/DPP Meeting, Chicago, Illinois, 8–12 November, 2010).
[51] L. L. Lodestro and L.D. Pearlstein, Phys. Plasmas **1** (1994) 90.
[52] M.A. Makowski & D. Ryutov, "X-Point Tracking Algorithm for the Snowflake Divertor", private communication.
[53] M.V. Umansky et al., "Analysis of geometric variations in high-power tokamak divertors." LLNL Report LLNL-JRNL-410565 (2009).
[54] V.A. Soukhanovskii, et al, Rev. Sci. Instrum. **83** (2012) 10D716.
[55] Y. Ou et al., Plasma Phys. Control. Fusion **50** (2007) 115001.
[56] C. Xu, et al., Transactions on Plasma Science **38** (2010) 163.
[57] J. Blum*, Numerical Simulation and Optimal Control in Plasma Physics*, Gauthier-Villars Series, Wiley, 1989.
[58] W. Zhu, et al., Phys. Rev. Lett. **96** (2006) 225002.
[59] J.-K. Park, et al, Phys. Rev. Lett **102** (2009) 065002.
[60] S.A. Sabbagh et al., Nuclear Fusion **50** (2010) 025020.
[61] A.C. Sontag, et al., Nuclear Fusion **47** (2007) 1005.
[62] M. Podesta and R. Bell, Rev. Sci. Intrum. **83** (2012) 10D903.

[63] K. Taira, et al., *Rotational Control of Plasma in NSTX*, American Physical Society, 51st Annual Meeting of the APS Division of Plasma Physics, November 2-6, 2009, #PP8.078
[64] H. Park, et al., Rev. Sci. Instrum **70** (1999) 710.
[65] J.-W. Juhn, et al. Rev. Sci. Instrum. **81** (2010) 10D540.
[66] B.P. LeBlanc, et al., Rev. Sci. Instrum **83** (2012) 10D527.
[67] R. Maingi, et al., Plasma Phys. Control Fusion **46** (2004) A305.
[68] V. Soukhanovskii, et al., Rev. Sci. Instrum. **75** (2004) 4320.
[69] D.L. Yu, et al., Nuclear Fusion **50** (2010) 035009.
[70] D. Lundberg, "*Fueling Studies on the Lithium Tokamak Experiment*", PhD. Thesis, Princeton University, 2012.
[71] S. P. Gerhardt, et al., "*On the Predictability of Disruptions in the High-β Spherical Torus NSTX*", submitted to Nuclear Fusion (2013).
[72] W.W. Heidbrink, et al, Nuclear Fusion **43** (2003) 883.
[73] T.C. Hender, et al., Nuclear Fusion **47** (2007) S128.
[74] J.W. Berkery, et al., *Global Mode Control and Stabilization for Disruption Avoidance in High-β ST Plasmas*, paper EX/P8-07, IAEA FEC, San Diego, CA (2012).
[75] H. Reimerdes, et al., Nuclear Fusion **13** (2006) 056107.
[76] D. Whyte, et al., Nuclear Fusion **50** (2010) 105005.
[77] A.E. Hubbard, et al., Phys. Plasmas **18** (2011) 080705
[78] H.Y. Yuh, et al., Phys. Rev. Lett **106** (2011) 055003.
[79] H. Yuh, et al., Phys. Plasmas **16** (2009) 056120.
[80] R. Maingi, et al. Phys. Rev. Lett. **105** (2010) 135004.
[81] E.D. Fredrickson, et al., Phys. Plasmas **16** (2009) 122505.
[82] W.W. Heidbrink, et al, Plasma Phys. Control. Fusion **51** (2009) 125001.
[83] K.L. Wong, et al., Phys. Rev. Lett **93** (2004) 085002.
[84] K. L. Wong, et al., Nuclear Fusion **45** (2005) 30.
[85] J.E. Menard, et al., *Progress on Developing the Spherical Tokamak for Fusion Applications,* paper FTP/3-4, IAEA FEC, San Diego, CA (2012).
[86] R. J. Hawryluk, et al., "An Empirical Approach to Tokamak Transport", in Physics of Plasmas Close to Thermonuclear Conditions, ed. by B. Coppi, et al., (CEC, Brussels, 1980), Vol. 1, pp. 19-46.
[87] L. L. Lao, Nuclear Fusion **25** (1985) 1611.
[88] See http://nstx-u.pppl.gov/software/lrdfit.
[89] S.A. Sabbagh, et al., Nucl. Fusion **41** (2001) 1601.
[90] A. Pankin, et al., Comput. Phys. Commun. **159** (2004) 157.